REPORT DOCUMENTATION PAGE

AFRL-SR-BL-TR-02-

0109

1. AGENCY USE ONLY (Leave blank)	2. REPORT DATE 03/06/02	3. REPORT Final (03/01/00 – 10/31/01)

4. TITLE AND SUBTITLE	5. FUNDING NUMBERS
Restoration and Super-Resolution of Diffraction-Limited Imagery Data by Bayesian and Set-Theoretic Approaches	F49620-00-1-0167

6. AUTHOR(S)

Dr. Malur K. Sundareshan

7. PERFORMING ORGANIZATION NAME(S) AND ADDRESS(ES)	8. PERFORMING ORGANIZATION REPORT NUMBER
Department of Electrical and Computer Engineering College of Engineering and Mines The University of Arizona Tucson, AZ 85721	

9. SPONSORING / MONITORING AGENCY NAME(S) AND ADDRESS(ES)	10. SPONSORING / MONITORING AGENCY REPORT NUMBER
AFOSR/NM 801 N. Randolph St. Room 732 Arlington, VA 22203-1977	

11. SUPPLEMENTARY NOTES

20020402 079

12a. DISTRIBUTION / AVAILABILITY STATEMENT

Approved for Public Release – distribution is unlimited

12b. DISTRIBUTION CODE

13. This project was primarily aimed at the design of novel algorithms for the restoration and super-resolution processing of imagery data to improve the resolution in images acquired from practical sensing operations. Due to the underlying diffraction limits, the image recorded at the output of the imaging system is usually a low-pass filtered version of the original scene and hence recovery of the lost information contributing to the finer details is required to produce resolution enhancement. Super-resolution algorithms attempt to provide not only passband restoration but also some degree of spectral extrapolation thus enabling to restore the high frequency spatial amplitude variations relating to the spatial resolution of the sensor and lost due to diffraction-limited imaging. These algorithms are typically iterative in nature and implement nonlinear signal processing operations. Two distinct approaches that have resulted in powerful super-resolution algorithms are based on statistical optimization arguments and set-theoretic estimation procedures. The principal objectives in this project were to develop and evaluate specific techniques for developing new processing algorithms by combining the strong points of the two approaches. The principal outcomes from this work include the following:

- Systematic procedures for extracting and modeling scene-derived information sets for projection-based set-theoretic super-resolution processing;
- Design of hybrid processing algorithms that integrate Projection Onto Convex Sets (POCS) iterations with Maximum Likelihood (ML) estimation procedures to yield superior restoration and super-resolution performance.

14. SUBJECT TERMS		15. NUMBER OF PAGES 58
		16. PRICE CODE

17. SECURITY CLASSIFICATION OF REPORT	18. SECURITY CLASSIFICATION OF THIS PAGE	19. SECURITY CLASSIFICATION OF ABSTRACT	20. LIMITATION OF ABSTRACT
UNCLASSIFIED	UNCLASSIFIED	UNCLASSIFIED	UNLIMITED

RESTORATION AND SUPER-RESOLUTION OF DIFFRACTION-LIMITED IMAGERY DATA BY BAYESIAN AND SET-THEORETIC APPROACHES

FINAL REPORT
(For AFOSR Grant # F49620-00-1-0167)

Prepared by: **Dr. Malur K. Sundareshan**
Professor of Electrical and Computer Engineering
University of Arizona
Tucson, AZ 85721-0104
Tel: (520) 621-2953; Fax: (520) 626-3144
e-mail: *sundareshan@ece.arizona.edu*

Prepared for: **Air Force Office of Scientific Research**
and
AF Wright Laboratory Armament Directorate

Program Manager: Dr. Jon Sjogren
AFOSR/NM, Arlington, VA 22203

November 30, 2001

RESTORATION AND SUPER-RESOLUTION OF DIFFRACTION-LIMITED IMAGERY DATA BY BAYESIAN AND SET-THEORETIC APPROACHES

FINAL REPORT

Dr. Malur K. Sundareshan
Professor of Electrical and Computer Engineering
University of Arizona, Tucson, AZ 85721-0104

ABSTRACT

This project, supported by a grant from the Air Force Office of Scientific Research, was primarily aimed at the design of novel algorithms for the restoration and super-resolution processing of imagery data to improve the resolution in images acquired from practical sensing operations. Due to the diffraction limits underlying these operations, the image recorded at the output of the imaging system is a low-pass filtered version of the original scene and hence recovery of the lost information contributing to the finer details is required to produce significant resolution enhancement. While traditional image restoration procedures (based on deconvolution and inverse filtering approaches) attempt mainly reconstruction of the passband, super-resolution algorithms attempt to provide not only passband restoration but also some degree of spectral extrapolation thus enabling to restore the high frequency spatial amplitude variations relating to the spatial resolution of the sensor and lost due to diffraction-limited imaging. These algorithms are typically iterative in nature and implement nonlinear signal processing operations. Two distinct approaches that have resulted in powerful super-resolution algorithms are based on statistical optimization arguments and set-theoretic estimation procedures. The principal objectives in this project were to develop and evaluate specific techniques for developing new processing algorithms by combining the strong points of the two approaches. The principal outcomes from this work include the following:

- Systematic procedures for extracting and modeling scene-derived information sets for projection-based set-theoretic super-resolution processing;
- Design of hybrid processing algorithms that integrate Projection Onto Convex Sets (POCS) iterations with Maximum Likelihood (ML) estimation procedures to yield superior restoration and super-resolution performance.

In order to increase the relevance of the work conducted in this project to the U.S. Air Force needs, a close liaison was maintained with the Air Force Wright Laboratory Armament Directorate (at Eglin AFB). For proof of concept demonstrations, the tailoring of the algorithms as well as the processing studies were conducted with a special focus on achieving resolution enhancements in the passive millimeter-wave (PMMW) images acquired by the Air Force Wright Laboratory Armament Directorate with the state-of-the-art radiometers being built by them.

TABLE OF CONTENTS

LIST OF FIGURES

4

1. INTRODUCTION

1.1   Principal Objectives of the Project

Imagery data acquired from practical sensing operations typically suffer from poor spatial resolution due to the finite size of antenna or lens that makes up the imaging system and the consequent imposition of the underlying diffraction limits. Hence, some form of post-detection image processing directed to enhancing the resolution will often be needed before the obtained measurements can be used reliably for any image exploitation and decision-making objectives. Image restoration has a considerably long history and several powerful procedures have been developed to restore degraded images [1]. However, since the image recorded at the output of the imaging system is a low-pass filtered version of the original scene, recovery of the lost information contributing to the finer details is indeed necessary to produce significant resolution enhancement. Recognizing this fact, researchers have directed their attention to the design of efficient processing schemes, commonly referred to as super-resolution algorithms, that achieve not only a satisfactory restoration of the passband (by attempting to reverse the effects of convolution with the sensor point spread function within the image bandwidth) but also some degree of spectral extrapolation to recover the lost frequencies beyond the diffraction-limited cutoff.

The primary goal in this project was the development of novel approaches and procedures for the restoration and super-resolution of diffraction-limited imagery data in order to achieve resolution enhancements that facilitate improved surveillance and tracking of targets of interest. In practical applications, potential advantages that could be achieved from such resolution enhancements beyond those dictated from practical limits (such as the one given by the Rayleigh criterion [2]) are:

5

(i) benefits in range of measurement – scene details that are potentially available from a closer range can be obtained from longer range measurements;

(ii) benefits in sensor dimensions – resolution levels that are potentially obtainable from a larger aperture or a bigger antenna can be achieved from less expensive or smaller size sensors (a typical payoff being to gain the effect of deploying a big antenna on a small airframe).

Our investigations towards this goal hence focused on several specific topics that included the following:

- development of novel approaches based on statistical modeling and convex constraint sets for resolution enhancement in the presence of noise and clutter;
- mathematical modeling of constraint sets and projection operators for specific *a priori* information about the object or scene being imaged in order to facilitate inclusion in the design of systematic restoration and super-resolution procedures based on the Projection-Onto-Convex-Sets (POCS) approach;
- investigation of methods for combining POCS-based approaches with maximum likelihood (ML) restoration methods for designing hybrid POCS-Bayesian super-resolution procedures;

Due to the fact that investigations on resolution enhancement have both military and non-military applications, the studies were conducted using a general framework and employing mathematical models. However, in order to provide validation of the studies conducted and the results obtained to military environments, the work was performed in close collaboration with the Air Force Wright Laboratory Armament Directorate personnel. In particular, the various simulation experiments conducted to demonstrate the efficiency of the algorithms developed in this project were appropriately tailored to process passive millimeter-wave (PMMW) imagery data acquired from state-of-the-art PMMW radiometers being built by the Advanced Sensors Group at the Air Force Wright Laboratory Armament Directorate.

1.2   Restoration and Super-resolution Processing of Sensor Acquired Data

Imaging sensors, no matter how carefully designed, have certain limitations arising mainly from physical constraints, the principal one being poor resolution in the acquired imagery. The diffraction-limited angular resolution, θ, of an incoherent imaging system [2] is given by

$$\theta = 1.22 \frac{\lambda}{D}$$

where λ is the effective wavelength of imaging and D is the diameter of the limiting aperture of the antenna or lens. As λ increases, the achievable angular resolution decreases, *i.e.* θ, the size of the angle between two resolvable points, increases. It may be noted that the wavelength of a synthetic aperture radar (SAR) operating at 1 GHz is about 1 inch long and one needs an antenna as big as 40 ft wide in order to achieve a resolution requirement of being able to able to distinguish points in a scene separated by about 1 meter at a distance of 1 Km. For a typical passive millimeterwave (PMMW) sensor with a 1 ft diameter antenna and operating at 95 GHz, the angular resolution is only about 10 mrad, which translates into a spatial resolution of about 10 meters at a distance of 1 Km. Some recent studies have also established that for ensuring reasonably adequate angular resolution (typically of the order of 4 mrad), a 95 GHz PMMW imaging system with a sensor depression angle of 60° - 80° needs to be confined to very low operational altitudes (of the order of 75-100 meters), which puts inordinate demands on the surveillance and guidance schemes to facilitate such requirements. Similar resolution limitations and the consequent requirements on operational conditions (some of which may be clearly impossible to satisfy for tactical missions with reliability and survivability constraints) exist for other types of sensing modalities as well. This in turn demands use of clever image processing techniques to process the acquired imagery data and obtain improved resolution in the processed

images.

The fundamental problem underlying the sensing operation is the "low-pass" filtering effect due to the finite size of the antenna or lens that makes up the imaging system and the consequent imposition of the underlying diffraction limits. Hence the image recorded at the output of the imaging system is a low-pass filtered version of the original scene. The portions of the scene that are lost by the imaging system are the fine details (high frequency spectral components) that accurately describe the objects in the scene, which also are critical for reliable detection and classification of targets of interest in the scene. Hence some form of image processing to restore the details and improve the resolution of the image will invariably be needed. Traditional image restoration procedures (based on deconvolution and inverse filtering approaches) attempt mainly at reconstruction of the passband and possibly elimination of effects of additive noise components. These hence have only limited resolution enhancement capabilities. Greater resolution improvements can only be achieved through a class of more sophisticated algorithms, called super-resolution algorithms, which provide not only passband reconstruction but also some degree of **spectral extrapolation**, thus enabling to restore the high frequency spatial amplitude variations relating to the spatial resolution of the sensor and lost through the filtering effects of the seeker antenna pattern. A tactful utilization of the imaging instrument's characteristics and any *a priori* knowledge of the features of the target together with an appropriately crafted nonlinear processing scheme is what gives the capability to these algorithms for super-resolving the input image by extrapolating beyond the passband range and thus extending the image bandwidth beyond the diffraction limit of the imaging sensor.

For application in surveillance environments, it must be emphasized that super-resolution is a post-processing operation applied to the acquired imagery and consequently is much less

expensive compared to improving the imaging system for desired resolution. As an example, it may be noted that for visual imagery acquired from space-borne platforms, some studies indicate that the cost of camera payload increases as the inverse 2.5 power of the resolution. Hence a possible two-fold improvement in resolution by super-resolution processing in this application roughly translates into a reduction in the cost of the sensor by more than 5 times. Similar relations also exist for sensors operating in other spectral ranges (due to the relation between resolution and antenna size), confirming the cost effectiveness of employing super-resolution algorithms. The principal goal of super-resolution processing in a multispectral surveillance environment is hence to obtain an image of a target of interest via post-processing that is equivalent to one acquired through a more expensive larger aperture sensor.

1.3   Basic Considerations in Design of Super-resolution Processing Algorithms

The idea of recreating the spectral components that are removed by the imaging process and hence are not present in the image available for processing may pose some conceptual difficulties, which may lead one to suspect whether super-resolution is indeed possible. Fortunately there exist sound mathematical arguments confirming the possibility of spectral extrapolation. The primary justification comes from the Analytic Continuation Theorem and the property that when an object has finite spatial extent its frequency spectrum is analytic [3]. Due to the property that a finite segment of any analytic function in principle determines the whole function uniquely, it can be readily proved that knowledge of the passband spectrum of the object allows a unique continuation of the spectrum beyond the diffraction limit imposed by the imaging system. It must be emphasized that the limited spatial extent of the object is critical in providing this capability for extrapolation in the frequency domain.

Fundamental to the reliable estimation of the high frequencies (that underly the super-resolution objectives) is the utilization of *a priori* known information during the processing steps. Indeed, since image restoration is inherently an ill-conditioned inverse problem, it is long realized that the quality of restoration and the extent of achievable super-resolution depend on the accuracy and the amount of *a priori* information the processing scheme can successfully employ. Some of the earliest procedures proposed for image super-resolution [4,5] are based on intelligently utilizing the known information in the form of constraints during the iterative processing steps. In practice, one finds that a lot of information typically exists to assist guiding the restoration process in a satisfactory direction. This includes, (i) *Information about the solution*, such as non-negativity of pixel intensities, spatial extent of objects present in the scene, known ranges for signal intensities, etc., (ii) *Information about the imaging system*, such as sensor phenomenology, aperture size and the resulting shape of the optical transfer function (OTF), etc., and (iii) *Information about the imaging conditions*, such as the extent of observation noise, object motion during imaging, etc. In addition, as will be shown in this paper, a variety of information can be extracted from the image that is being processed, which we will call *scene-derived information*, and this can further assist in the restoration operations.

Does availability of more information automatically translate into better restoration and more super-resolution? Since the primary objective is the creation of data not present in the image being processed, there is major concern on the fidelity of the estimated high frequencies (one may note that addition of random noise can also lead to an expansion of image bandwidth). Utilization of more and diverse types of information consequently provides a mechanism for cross-validation thus resulting in a faithful re-creation of the true frequencies present in the object or scene being restored. Employing all of the available information does not come

without a price, however. More information used during the iterative processing steps almost always translates into increased computational complexity, which in turn could contribute to poorer convergence speed of the super-resolution algorithm. It is easy to see that if two different types of information that are desired to be utilized are not appropriately modeled for inclusion in the algorithm (as an example, two information sets modeled such that they do not have a proper intersection), it will have detrimental effects on the algorithm convergence. Consequently, information analysis and information modeling are critical steps before subjecting the image to super-resolution processing.

Varying by the extent to which *a priori* knowledge can be incorporated in algorithm development, there have been introduced into the literature a large number of image restoration approaches and algorithms too vast to describe or reference here. One may refer to some recent survey papers [6,7] for a review of the extensive activity on this topic. In the context of the objectives of the present project however, it is important to recognize that only a small subset of the approaches that are developed for image restoration have received some interest for their super-resolution capabilities, i.e. possible spectrum extrapolation performance. One may note that not all image restoration methods provide the capability for super-resolving. In fact, a majority of existing schemes may perform decent passband restoration, but provide no bandwidth extension at all.

The various approaches in general attempt to code the *a priori* knowledge to be used by specifying an object model or a set of constraint functions, and further employ an appropriate optimization criterion to guide in the search for the best estimate of the object. A convenient way of classifying the resulting algorithms is into **iterative** and **noniterative** (or direct) schemes. Fig. 1a and 1b depict schematically these two basic approaches. Noniterative approaches generally

11

attempt to implement an inverse filtering operation (without necessarily performing the computation of the inverse of the PSF matrix H, however) and have poor noise characteristics. All required computations and any possible use of constraint functions are applied in one step. In contrast, iterative methods apply the constraints in a distributed fashion as the solution progresses and hence the computations at each iteration will be generally less intensive than the single-step computation of noniterative approaches. Some additional advantages of iterative techniques are that, (1) they are more robust to errors in the modeling of the image formation process (uncertainties in the model for the sensor point spread function, for instance), (2) the solution process can be better monitored as it progresses, (3) constraints can be utilized to better control the effects of noise (and possibly clutter), and (4) can be tailored to offset sensor nonlinearities. The disadvantages of these methods generally are, (1) increased computation time, and (2) need for proving convergence of the iterative scheme. Despite these disadvantages, iterative methods are generally the preferred approach due to their numerous advantages and also since the iteration can be terminated once a solution of a reasonable quality is achieved. Consequently, most of the research in tailoring super-resolution algorithms is taking place at present times in formulating iterative procedures.
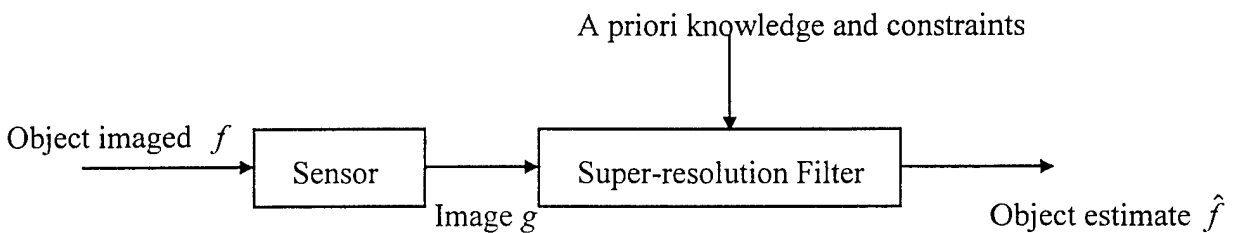

Fig. 1a. Schematic of Noniterative (Direct) Super-resolution

Object imaged f — Super-resolution Processing
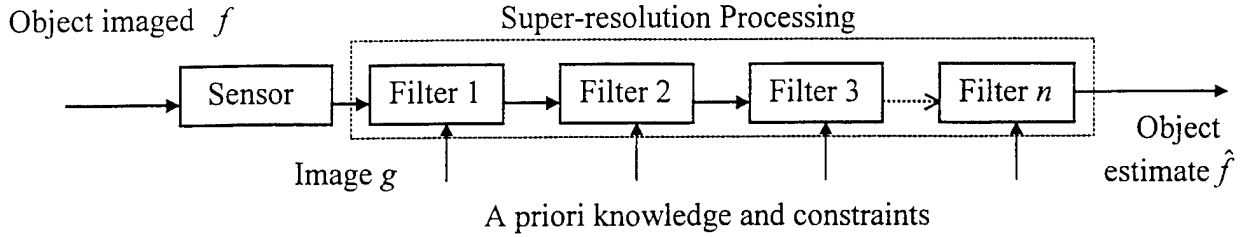
Fig. 1b. Schematic of Iterative Super-resolution

1.4   Approaches and Methods for Design of Super-resolution Algorithms

For the design of specific digital processing algorithms for image super-resolution, a number of different approaches have been proposed in the past, which have lead to explicit procedures for both iterative and non-iterative constructions of the restored image from its degraded version. Perhaps one of the earliest procedures, suggested by Gerchberg [4] and Papoulis [5], involves alternately applying constraints in the space-domain and in the frequency-domain in the quest for reconstructing the unknown portion of the frequency spectrum from a limited known portion, *viz.* the passband of the sensor. Much of the activity in recent times has centered on statistical optimization methods. In this approach one employs an iterative scheme for constructing estimates of the object imaged, either in the form of a maximum likelihood (ML) estimate [8-10] or a maximum a posteriori (MAP) estimate [11-13], from using the acquired image and an OTF model for the sensor. A specific iterative updating scheme, which is a special form of implementing the well known Expectation-Maximization (EM) algorithm and is popularly referred to as Richardson-Lucy iteration, attempts to improve the value of the likelihood function during successive iterations. This scheme has received considerable attention in the past and several studies (too numerous to mention individually) have been directed to understanding the convergence and other properties of the iterative process. Several modifications and refinements of these algorithms have also been developed in the recent past to ensure good performance even under non-ideal conditions such as imperfect knowledge of

sensor OTF and high levels of noise corrupting the acquired image [14,15]. A few non-iterative algorithms have also been developed. Notable among these is the algorithm due to Darling *et al.* [16], which performs regularized approximation in a weighted Hilbert space by utilizing *a priori* information. A more recent effort in this direction is due to Walsh and Nielsen-Delaney [17] who employed a method based on singular value decomposition. It is generally agreed, however, that non-iterative methods do not offer the same degree of flexibility provided by iterative methods in utilizing the known *a priori* information during processing, which is at the heart of super-resolution constructions. Extensive comparison studies that document the performance benefits resulting from the use of iterative algorithms when compared with other approaches for the super-resolution processing of specific types of images are also available [18,35].

The effectiveness of statistical optimization methods in achieving restoration and super-resolution depends to a large extent on the probability distribution models used to formulate the optimization criterion (i.e. the probability model for the likelihood function or for the *a posteriori* distribution). For the sake of obtaining a simple–to-implement updating algorithm, one typically employs a simple distribution function, such as a Poisson process, to model these quantities. Unfortunately however, processing with such an algorithm can yield less than optimal performance when the emission process underlying the particular sensing mechanism deviates from Poisson statistics and requires a more general distribution model (such as a Rayleigh distribution). Use of more general distribution functions in the optimization process will result in corresponding iterative updating schemes, which may not be attractive to implement due to heavy computational demands. Thus, there is a fundamental conflict between the goals of *implementation simplicity* and *accuracy of representation* in the design of algorithms following this approach forcing one to sacrifice one or the other of the two objectives.

14

Yet another approach for image restoration that is gaining greater popularity but is fundamentally very distinct from the statistical optimization methods is the employment of a convex set theoretic framework in which several constraint sets that could be formulated from known *a priori* information can be employed during iterative processing steps. When compared to statistical methods for image restoration, set-theoretic methods are relatively new. The earliest work on set-theoretic estimation in a general context can be traced to a 1965 paper by Bergman [19]. The Gerchberg-Papoulis procedure for super-resolution [4,5], discussed earlier, can be regarded as another early attempt at implementation of set-theoretic estimation to signal reconstruction. However, it is the introduction of a new iterative procedure for an organized synthesis of set theoretic estimates, which has now come to be known as *Projection Onto Convex Sets* (POCS), that marked the beginning of the interest in this approach and secured its steady growth. Although the POCS framework was first developed by Gubin *et. al.* [20], and further expanded by Lent *et. al.* [21], it was a series of three pioneering papers by Youla and others [22-24] that popularized this approach among the scientific and engineering community and established a broad conceptual and computational basis for signal recovery. Some useful properties of POCS reconstructions in the solution of deconvolution problems are also discussed by Trussell and Civanlar [25]. A comprehensive discussion on this approach together with several useful extensions can be found in a tutorial paper by Combettes [26]. In the field of image processing, more interest in this approach has so far been shown by medical imaging researchers in handling such problems as tomographic image reconstruction [27,28] and construction of 3-D animations of cardio-vascular functions [29], etc.

The conflict cited above that exists between *implementation simplicity* (which in turn is motivated by the desire to execute sufficient number of algorithm iterations in real time without

slowing the output rate of sensor) and *representation accuracy* (which is motivated by the desire to utilize as much of the relevant and accurate information as feasible during the processing steps) has encouraged researchers to seek new methods that enable one to handle the trade-offs more satisfactorily. In this report we shall present an attractive solution towards this goal by attempting to answer the question – "how can the super-resolution performance of a simple-to-implement algorithm, such as the Richardson-Lucy iteration, be improved by use of additional knowledge that may be available?" An answer to this question is suggested by the inclusion of intermediate adjustment steps involving implementation of convex constraint sets that model the available additional knowledge. Motivating the development of the resulting processing schemes is the observation that set theoretic methods offer a greater flexibility in incorporating available *a priori* information into the restoration process than what one can achieve by attempting to squeeze all of this information into a single probability distribution function used in the statistical optimization process. The restoration of the degraded image is achieved by iteratively projecting the image onto the various convex constraint sets that model the different types of *a priori* information one may have in the restoration problem at hand. While efforts at the modeling of constraint sets and the use of these in projection-based set theoretic image recovery constitutes a popular direction for research at present, it seems that the idea of combining the strong points of Bayesian schemes and that of the convex set based methods has not received much attention. In fact, development of processing algorithms that intelligently combine the strong points of Maximum Likelihood and POCS approaches has not been addressed at all. A primary contribution of this project is the design of hybrid algorithms that attempt to leverage the strong points of both ML iteration scheme (simplicity of execution, known convergence properties, etc.) and the POCS adjustments (utilization of diverse types of information in guiding the restoration

process, faster decay of restoration error, etc.). The development of specific constraint sets that model the scene-derived information for use in the POCS adjustment steps constitutes yet another important contribution of this work.

1.5   Outline of the Report

The organization of this report is as follows. In Section 2 we discuss some basics of the ML restoration algorithm and describe its super-resolution performance when applied to blurred images. A mathematical analysis of the dynamics of the iterative process is presented to give an insight into the properties of the restored image as well as to gain an understanding of the possible modifications to improve the super-resolution performance. In Section 3 we give a brief description of the mathematical background for set-theoretic image recovery. We also propose two novel information extraction and constraint set modeling schemes, and their application in a set theoretic image recovery framework. In Section 4 we present a new hybrid approach that is tailored to combine the strong points of a Bayesian scheme, such as the ML algorithm, and those of a projection based set-theoretic restoration scheme. Finally, we describe the performance of two new super-resolution algorithms following this approach by presenting results of a few experiments of super-resolving degraded image data. In order to emphasize the application of these algorithms in the super-resolution of diffraction-limited images acquired in practice, we will specifically include results from experiments of processing passive millimeter-wave images acquired at the 95 GHz range[1] from state-of-the-art millimeter-wave radiometers. Finally in Section 6, we shall present a summary of the results accomplished during this project and offer some concluding remarks.

---

[1] It is to be noted that at these frequencies the signals have tremendous penetrating power thus providing attractive imaging capabilities under adverse conditions and consequently a great interest exists at present in developing passive sensors operating at these frequencies. However, due to Rayleigh diffraction limits, the resolution in the acquired image will be very poor offering the greatest challenges to test the ability of restoration and super-resolution algorithms.

2. SUPER-RESOLUTION BY ITERATIVE MAXIMIZATION OF LIKELIHOOD

2.1 Restoration and Super-resolution Performance of an Iterative ML Algorithm

As noted earlier, iterative image restoration algorithms developed using a maximum likelihood (ML) estimation framework have attained considerable significance in recent times for their super-resolution capabilities. The basic idea underlying these methods is to account for the statistical behavior of the emitted radiation at the level of individual photon events by constructing appropriate object radiance distribution models. An algorithm that affords a convenient digital implementation can be developed starting from a discretized formulation of the model for the imaging process

$$g(y) = \sum_{x \in X} h(y,x) f(x) + n(y) \tag{1}$$

where $f(x)$ denotes the object's intensity function defined on a region X, $g(y)$ denotes the intensity detected in the image defined on a region Y and $h(x, y)$ denotes the point spread function (PSF) of the imaging sensor and $n(y)$ denotes the noise present. The classical image restoration problem is to find the object intensity estimate $f(x)$ given the data $g(y)$.

There exists considerable literature on developing explicit algorithms, mainly of an iterative nature, for handling the image restoration problem within a statistical framework afforded by such a formulation. A particularly attractive approach is to obtain a ML estimate $\hat{f}(x)$, i.e. the object intensity estimate that most likely have created the measured data $g(y)$ with the PSF process $h(y,x)$, which in turn is developed by maximizing an appropriately modeled likelihood function. Modeling the likelihood function is basically obtaining a goodness-of-fit (GOF) quantity for the measured data, since the likelihood function is a statistical distribution function $p(g/f)$ obtained as a fit to the relation between the data $g(y)$ and the object $f(x)$.

For obtaining a digital processing algorithm, assuming that the image to be processed consists of $M \times M$ equally spaced gray level pixels obtained through a sampling of the image field at a rate that satisfies the Nyquist criterion, and using a lexicographical ordering of the signals g, f and n, one can rewrite (1) as a convolution of two one-dimensional vectors $h = [h(1), h(2), ..., h(N)]^T$ and $f = [f(1), f(2), ..., f(N)]^T$ in the form

$$g(i) = h(i) \otimes f(i) + n(i), \qquad i = 1, 2, ..., N, \tag{2}$$

where $N = M^2$ and $\otimes$ denotes convolution. Now assuming a Poisson distribution for $p(g/f)$, the estimate of the object $\hat{f}(x)$ that solves the optimization problem

$$\hat{f} = \arg \max_f p(g/f) \tag{3}$$

can be developed through an iterative updating scheme given by

$$\hat{f}_{k+1}(j) = \hat{f}_k(j) \left[\left\{ \frac{g(j)}{\hat{f}_k(j) \otimes h(j)} \right\} \otimes h(j) \right] \tag{4}$$

where $\hat{f}_k(j)$ denotes the estimate of $f(j)$ constructed at the kth iteration and $\otimes$ denotes discrete convolution. Details on the derivation of this algorithm can be found in the literature [4,5].

The ML algorithm outlined above possesses some attractive features (such as guaranteed convergence, non-negativity of estimates, etc.) that are useful in practical implementation. The optimization framework in which the algorithm is developed ensures that the likelihood function $p(g/f)$ monotonically increases over successive iterations of the algorithm and hence the processed image improves in quality as the algorithm proceeds.

For demonstrating the super-resolution capabilities of this algorithm, some representative results of applying it to restore blurred images is shown in Figs. 1 and 2. In Fig. 1a is shown the blurred version of a simulated object comprising of a series of concentric disks created with the

background (dark) at intensity value zero and the disks (bright) at intensity value one. For simulating the blurring caused by a diffraction limited imaging sensor, this object was convolved with the PSF of a low pass filter, with the result shown in Fig. 2a. In Fig. 2b is shown the restored version of this image, and as is evident, the processing removes most of the effects of blurring thus attempting to restore the original object. To demonstrate the extent of super-resolution achieved, the magnitude spectra of the blurred image and the restored image are shown in Figs. 3a and 3b respectively. The expanded frequency content clearly attests to the super-resolution performance of the algorithm.

1a   1b
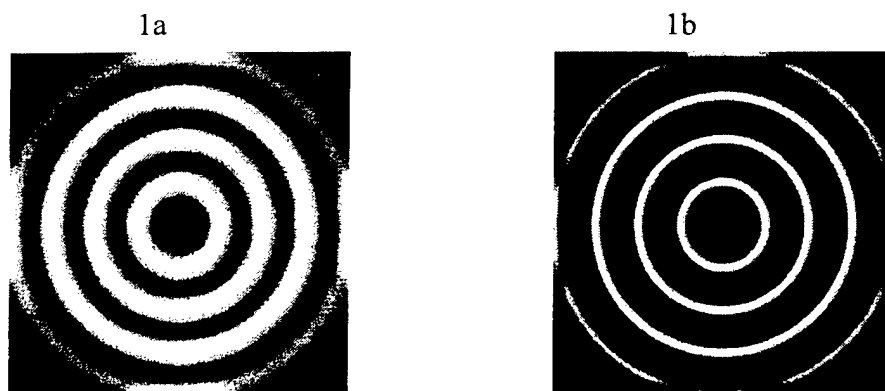

Figs. 2a and 2b: Blurred "Circles" image and its restoration by ML algorithm

2a   2b
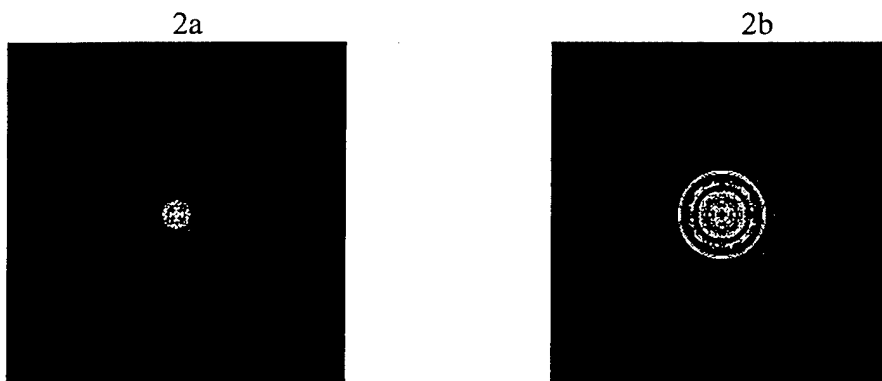
Figs. 3a and 3b: Magnitude spectra of blurred and restored Images

To illustrate the restoration achievable in processing practically acquired images with this algorithm, the results of an experiment are presented. Fig. 4a shows a PMMW image ("Tank

Image") acquired by a single detector radiometer with 1 ft diameter aperture operating at 95 GHz. Figs. 4b and 4c respectively show the restored images obtained at the end of 25 and 100 iterations. It is evident that the resolution has considerably improved and the algorithm is quite powerful in producing an image from which better features can be extracted than from the original for any further information exploitation analysis, such as target classification. For facilitating real-time implementation capability however, one desires to reduce the number of iterations needed to obtain this level of resolution improvement, or to achieve even better resolution if possible with less computational overhead. As will be shown later in this paper, the POCS-assisted ML algorithm developed here will provide this capability.
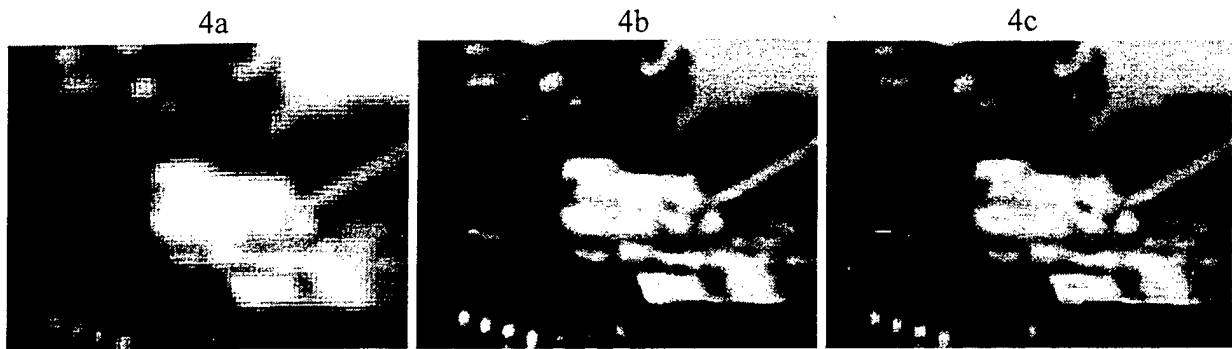
Figs. 4a, 4b and 4c: Acquired PMMW image and its super-resolved versions after 25 and 100 iterations of ML algorithm

2.2   Analysis of the Dynamics of the Iterative Scheme

Although the restoration and super-resolution performance of the algorithm described in Eq. (4) appear quite impressive from the experimental results presented above, an analysis of the dynamics of the iterations is useful to obtain a greater insight into the restoration performance. In the simulation experiment whose results are shown in Figs. 2 and 3, the original object ("Circles" image from which the blurred version was constructed) is known, and hence a plot of the "restoration error" (measured as some appropriate norm of the deviation between the original object and the restored image) as iterations are continued can provide an indication of the speed

21

of convergence of the algorithm. Also, since the algorithm is developed employing a maximum likelihood framework, at each successive iteration the value of the likelihood function can be computed from noting that the logarithm of the likelihood function is given by

$$L(g\,/\,f) = \ln p(g\,/\,f) = \sum_{k=1}^{N}\left[g_k \ln\!\left(\sum_{j=1}^{N} h_{kj} f_j \right) - \sum_{j=1}^{N} h_{kj} f_j \right],\tag{5}$$

and this provides an alternate way of displaying the dynamics of the iterative scheme. Figs. 5a and 5b respectively show the behavior of the L_2-norm of the deviation between the object and the processed image, and the increase in likelihood, as iterations progress. It can be seen that the two curves display an inverse behavior, which is to be expected. What is more interesting, however, is to observe that after an initial steep decay of the restoration error, or a steep increase in the likelihood, the changes in the values of these quantities between two successive iterations get progressively less pronounced. A more rigorous mathematical analysis of the iterative scheme is useful to gain further insight into this behavior.
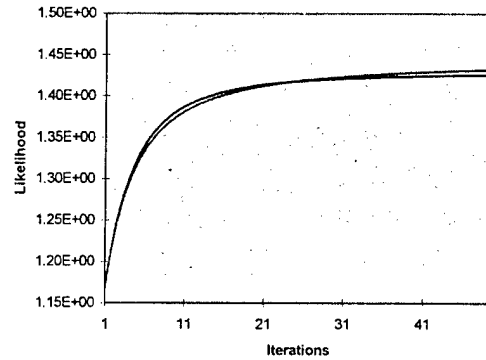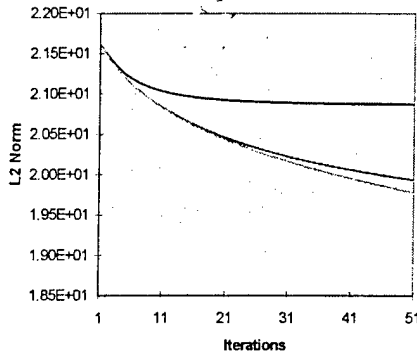
Fig. 5a. Convergence of restoration error   *Fig. 5b. Likelihood increase with progress of iterations*

22

The ML iterations specified by Eq. (4) result in a nonlinear dynamical process of the form

$$\hat{f}_{k+1}(j) = \Phi\big(\hat{f}_k(j)\big) \tag{6}$$

where $\Phi\big(\hat{f}_k(j)\big) = \hat{f}_k(j)\left[\left\{\dfrac{g(j)}{\hat{f}_k(j)\otimes h(j)}\right\}\otimes h(j)\right]$. The convergence of the iterations can hence

be examined in terms of the equilibrium points of this dynamical system, or equivalently of the

"fixed points" $\hat{f}_k(j)$ that satisfy

$$\Phi\big(\hat{f}_k(j)\big) = \hat{f}_k(j). \tag{7}$$

It is easy to see that this condition is attained at the k-th iteration when the restored image

satisfies the equality

$$g(j) = \hat{f}_k(j)\otimes h(j),$$

since the quantity inside the square brackets in the description of $\Phi\big(\hat{f}_k(j)\big)$ becomes 1 (when the

PSF is symmetric and normalized, which in turn implies that $1\otimes h(j) = 1$). Let the image

estimate vector $\big\{\hat{f}^*(j)\big\}$ denote this converged value. Thus

$$g(j) = \hat{f}^*(j)\otimes h(j) \tag{8}$$

specifies the fixed points $\big\{\hat{f}^*(j)\big\}$ of the ML restoration algorithm given by Eq. (2).

A careful examination of the condition specified by Eq. (8) reveals several interesting

facts. First of all observe that it corresponds to the condition in the frequency domain

$$G(j\omega) = \hat{F}^*(j\omega)H(j\omega) \tag{9}$$

and hence is satisfied by any estimate $\big\{\hat{f}^*(j)\big\}$ that restores the passband spectrum. Due to the

band-limiting operation of the convolution with the PSF vector $\big\{h(j)\big\}$, the image estimate

$\left\{\hat{f}^*(j)\right\}$ that satisfies Eq. (6) is not unique. Since equality outside the passband of the sensor is trivially satisfied (*i.e.,* both the left and the right sides of Eq. (9) become zero), there exist an infinite number of vectors $\left\{\hat{f}^*(j)\right\}$ that make Eq. (10) hold. These vectors are however related in the sense that each of them has a specific structure that permits it to be written as the sum of a fixed vector $\left\{\hat{f}^*_{pb}(j)\right\}$ that matches the object spectrum $F(j\omega)$ identically below the diffraction limit (*i.e.,* for $\omega \le \omega_c$) and another vector $\left\{\hat{f}^*_{sb}(j)\right\}$ with arbitrary values but with the spectrum below the diffraction limit identically zero. In other words, any estimate $\left\{\hat{f}^*(j)\right\}$ that can be written as

$$\hat{f}^*(j) = \hat{f}^*_{pb}(j) + \hat{f}^*_{sb}(j) \tag{10}$$

where $\hat{f}^*_{pb}(j)$ and $\hat{f}^*_{sb}(j)$ satisfy the frequency-domain conditions:

$(i) H(j\omega)\hat{F}^*_{pb}(j\omega) = G(j\omega)$

$(ii)\hat{F}^*_{sb}(j\omega) = 0 \qquad$ for $\omega \le \omega_c$, $\tag{11}$

serves as a fixed point of the ML algorithm.

It is now simple to note that the ML algorithm that iteratively strives to maximize the likelihood of the estimate $\left\{\hat{f}_k(j)\right\}$, which gives rise to the image vector $\left\{g(j)\right\}$ upon convolution with the PSF vector $\left\{h(j)\right\}$, attempts to enforce the passband restoration condition given by (*i*) above. Hence, when an estimate $\left\{\hat{f}_k(j)\right\}$ that satisfies this condition is obtained at the *k*-th iteration, the algorithm ceases to do any further work. Consequently, convergence of the algorithm is to be interpreted only in terms of restoration of the passband spectrum of the image. In other words, these algorithms principally strive to restore the passband as accurately as possible with the following resultant effects:

24

(i) Since there is no special incentive for obtaining the part $\left\{\hat{f}_k^{sb}(j)\right\}$ that matches the object spectrum outside the diffraction limit specified by ω_c, this vector obtained at the end of several iterations (when convergence has occurred) could have elements whose contribution to the frequency spectrum is much smaller than the contribution of the other part $\left\{\hat{f}_{pb}^*(j)\right\}$. In other words, the "energy in the frequency extension" could be very small (or even negligible).

(ii) When passband restoration is completed (*i.e.,* when convergence has occurred), no further changes in the estimate $\left\{\hat{f}_k(j)\right\}$ are likely, since the likelihood function will have attained its maximum value.

The analysis given above of the convergence behavior of the ML iterations is very helpful in obtaining an insight into the nature of the multiple fixed points of the algorithm and the effects of processing digital imagery data. Due to the infinite number of fixed points and the corresponding trajectories that describe the convergence of the initial estimates to these equilibrium conditions, obtaining any quantitative estimates of the convergence rates is rather difficult. The problem can be somewhat simplified by examining the dynamics of the "iteration error', or change in the estimate during successive iteration steps, defined by

$$e_k(j) = \hat{f}_k(j) - \hat{f}_{k-1}(j).$$ (12)

The behavior of this error is governed by the nonlinear dynamical process

$$e_{k+1}(j) = \hat{f}_{k+1}(j) - \hat{f}_k(j) = \Phi\left(\hat{f}_k(j)\right) - \hat{f}_k(j)$$ (13)

which can be re-written as

$$e_{k+1}(j) = \Psi\left(e_k(j)\right)$$ (14)

25

by expressing $\hat{f}_k(j)$ in terms of $e_k(j)$. Eq. (14) represents a nonlinear dynamical system whose trajectory behavior starting from an initial state $e_0(j) = \hat{f}_0(j) = g(j)$ is of interest. The equilibrium points of this "error system" are at the locations where $\Psi(e_k(j)) = 0$, which implies $\Phi(\hat{f}_k(j)) - \hat{f}_k(j) = 0$, and hence $e_{k+1}(j) = 0$. Thus the multiple fixed points of the ML algorithm $\{\hat{f}^*(j)\}$ (on the N-dimensional space for the estimate $\hat{f}$) are mapped into the unique equilibrium point $\{e(j) = 0\}$, which is the origin of the N-dimensional space for the iteration error. Hence the convergence rate for the restoration can be studied in terms of the trajectory behavior of the "error system" given by Eq. (14) near this equilibrium point.

For small values of $e_k(j)$ (i.e., near convergence to this equilibrium), $\Psi(e_k(j))$ can be linearized by a Taylor series in the form

$$\Psi(e_k(j)) = Je_k(j) + \ [\text{ Higher Order Terms }] \tag{15}$$

where J is the $N \times N$ Jacobian matrix $J = \partial\Psi / \partial e_k$. Ignoring the Higher Order Terms in the expansion, the iteration error dynamics can now be approximated by the linear system

$$e_{k+1}(j) = Je_k(j). \tag{16}$$

Solving this system of equations yields the trajectory behavior on the N-dimensional error space which can be described by

$$e_k(j) = J^k e_0(j) \tag{17}$$

where J^k is the state transition matrix of the system and $e_0(j)$ specifies the starting error.

From the convergent nature of the ML algorithm it follows that all eigenvalues of J are inside the unit circle, i.e., $|\lambda_i(J)| < 1$ where $\lambda_i(J)$, $i = 1,2, \ldots, N$, denote the eigenvalues of J. Consequently, the rate of decay of the error $e_k(j)$ is larger during the first few iterations of the

26

algorithm and progressively flattens as the number of iterations grow, a fact that was confirmed by the simulation experiments earlier. As will be observed later, this provides the motivation to introduce appropriate adjustment steps after executing a few iterations of the ML algorithm in order to re-gain a sharper decay of the error by re-playing the commencement phase of the ML algorithm several times.

3. POCS APPROACH TO RESTORATION WITH SCENE-DERIVED INFORMATION CONSTRAINTS

3.1 Basics of Convex Set-theoretic Restoration of Images

An approach that runs parallel to but is very distinct from the statistical optimization method used in deriving the ML algorithm is the employment of a convex set theoretic framework in which several constraint sets that could be formulated from known *a priori* information could be utilized. In order to highlight the differences between the two approaches, starting once again with the discretized model of the imaging process given by Eq. (1), the primary objective is to model each piece of prior information Ψ_i that is known as a closed convex constraint set S_i and seek an estimate $\hat{f}$ of the object by solving the optimization problem

$$\hat{f} = \arg\min_f \sum_{i=1}^{L} w_i J_i(\hat{f}, S_i) \tag{18}$$

where L denotes the number of constraints defined, w_i are a set of weights, and $J_i(\hat{f}, S_i)$ denotes a proximity measure that determines how well the current estimate satisfies the ith constraint. The proximity measure can be uniquely defined for a convex constraint scenario as [26]

$$J_i(\hat{f}, S_i) = \min_{f_p \in S_i} \left\| \hat{f} - f_p \right\|^2 \tag{19}$$

where $f_p = P_i(\hat{f})$ denotes the projection of $\hat{f}$ onto the set S_i. It is evident that the measure defined above quantifies deviations in the image domain; one can alternately use corresponding measures that quantify deviations in the frequency domain in order to reflect more explicitly the objectives of super-resolution.

The projection operators are non-linear mappings with several analytical properties which can be exploited to develop iterative set-theoretic algorithms for image restoration. Although

28

several algorithms were developed as early as in the late thirties, the potential of convex set-theoretic methods in image restoration has come to be appreciated since the advent of the method of projection onto convex sets (POCS) [22-24].

For a brief description, the first step in applying the method of POCS to an image recovery problem is to define a closed convex set for each of the *a priori* constraints in such a way that the members of the set are consistent with the associated constraint and each set contains the actual image distribution. An estimate of the image distribution is then defined to be any member of the intersection of the constraint sets. Finding an estimate by POCS is then equivalent to the problem of finding a point in the intersection of a number of closed convex sets.

Suppose that we have several *a priori* known constraints that can be associated with closed convex sets C_i, $i = 1, 2,..., L$, and let their respective projection operators be denoted P_i. Then the estimate $\hat{f}_n$ generated at the nth iteration by a sequential application of the projections on the previous iterate $\hat{f}_{n-1}$, *i.e.*

$$\hat{f}_n = P_m P_{m-1} P_{m-2} \text{...........} P_1 \hat{f}_{n-1} \tag{20}$$

converges to an estimate $\hat{f}$ in the intersection set $C_0 = C_1 \cap C_2 \cap C_3 \text{.........} \cap C_m$. It is further demonstrated [26] that a faster convergence to an estimate $\hat{f}$ lying within the intersection set can be achieved if instead of using the projection operators P_i in the construction of the estimate, one uses "relaxed projections" T_i, $i = 1, 2, ..., m$ defined by

$$T_i = (1 - \lambda)I + \lambda P_i \tag{21}$$

where λ is a parameter suitably selected within the range $0 < \lambda < 2$ and the estimate $\hat{f}$ is constructed iteratively by implementing the algorithm

$$\hat{f}_n = T_m T_{m-1} T_{m-2} \cdots\cdots\cdots T_1 \hat{f}_{n-1}. \tag{22}$$

For evaluating the performance of these algorithms an appropriate metric is the normalized proximity function given by

$$\Phi_n = 10\log \frac{\sum_{i=1}^{m} w_i J_i(\hat{f}_n, S_i)}{\sum_{i=1}^{m} w_i J_i(\hat{f}_0, S_i)}. \tag{23}$$

where w_i are weights selected suitably in proportion to the relative importance of the proximities to individual constraint sets the final estimate is desired to satisfy.

The projection operations executed in a serial manner as described in Eq. (20) (or in Eq. (22)) corresponds to enforcing the constraints in a sequential manner. In practice, one may gain considerable computational time benefits by applying the projections in parallel and constructing the estimate as a weighted sum of the individual projections as will be described later.

3.2 Scene-derived Information and Constraint Set Modeling

Due to the ill-posed nature of the super-resolution problem, it is essential to use as much prior information as we can have in order to make the solution more and more well conditioned. It is here that lies the advantage of projection based convex set-theoretic methods. POCS based image recovery schemes are extremely flexible. We can incorporate any *a priori* information as long as there exists a mathematically tractable projection operator for evaluating the set estimates. For example if we have the prior knowledge about the location of object boundaries, then we can model it as a convex constraint set and restore the object boundary edges. Such restoration of the object boundaries is of particular interest in super-resolution as we would be restoring the high frequencies corresponding to the object boundary edges.

Utilization of prior information for convex set-theoretic super-resolution of images can be thought of as a two-step process. In the first step we try to extract appropriate information for the image to be restored. The second step is primarily involved in the subsequent modeling of that information in the form of a convex set. The main challenging aspect of this exercise is the extraction of reliable information from given images. Constraint sets that have traditionally been used in image restoration by POCS formulations are non-negativity of intensity estimates, known spatial limits on objects in the scene, and variance of noise present in the scene being estimated, all of which are fairly easy to model as convex sets [28]. We will now present the development of two new constraint sets that can be formulated by performing simple pre-processing operations on the image being restored.

Border Constraint Set:

In several scenes of interest, objects of interest will be superimposed as foreground against a primarily flat background. Thus, a sharp transition in gray level intensity exists in the actual scene imaged. Due to blurring caused by the sensor, this sharp edge will be lost and image energy from foreground region flows into the background pixels, thus making it difficult to decide exactly where the foreground ends and the background begins. Thus, if one can determine the spatial extent of the object, or the border pixels bounding the object, one can sharpen the edge between the foreground and the background. In the spectral domain, this sharpening corresponds to recovering the higher frequency components, and hence super-resolution.

Any border extraction algorithm based on edge detection processing can be used for developing constraint sets that permit a foreground-background separation of the image, a popular one being Canny's edge detector [30]. This is a gradient-based scheme which attempts to design the edge detector by employing an optimization framework in order to achieve the

31

following objectives: (i) maximize the signal-to-noise ratio, (ii) achieve good localization to accurately mark edges, and (iii) minimize the number of responses to a single edge.

A version of this scheme that is particularly suited for the present purposes of building a constraint set for POCS restoration will now be outlined. The basic idea behind the procedure is to find the maximum of the partial derivative of the image f in a direction orthogonal to the edge orientation. To execute this task, one can create a two-dimensional mask for the edge orientation by convolving a linear edge detection function aligned normal to the edge direction with a projection function aligned parallel to the edge direction. A substantial computational savings results if both functions are chosen to be Gaussian with the same standard deviation σ such that the mask can be created by differentiating normal to the edge orientation as

$$G_n = \frac{\partial G}{\partial n},$$

(24)

where G is the two-dimensional symmetric Gaussian function $G = \exp\left(-\frac{x^2 + y^2}{2\sigma^2}\right)$. Ideally, n should be oriented normal to the edge direction, and although this direction is not known a priori, one can form a good estimate from the smoothed gradient direction

$$n = \frac{\Delta(G \otimes f)}{\|\Delta(G \otimes f)\|},$$

(25)

where $\otimes$ denotes convolution. An edge point is then defined to be a local maximum (in the direction of n) of the operator G_n, which is characterized by $\frac{\partial}{\partial n} G_n \otimes f = 0$, or equivalently

$$\frac{\partial^2}{\partial n^2}(G \otimes f) = 0.$$

(26)

Gaussian smoothing is now done by filtering the image with a Gaussian sliding window, with the window size generally chosen to be 6σ with the two dimensional Gaussian being centrally located. The resulting filtered version is obtained by placing this mask and performing a weighted addition of the pixels which lie within the window, with the weight for any pixel chosen as the value of the Gaussian at that location. In addition to smoothing, this step also helps in reducing the number of spurious edges due to noise that may be present in the image. A judicious selection of the value of σ provides the desired amount of smoothing, with larger values providing correspondingly more smoothing. For most images, we found that a value of σ selected in the range 0.5 to 2 provides a good choice.

From the smoothed image, one can easily compute the magnitude and the direction of the gradient as

$$\Delta f(i,j) = \frac{\partial f(i,j)^2}{\partial x} + \frac{\partial f(i,j)^2}{\partial y} \quad \text{and} \quad \Theta f(i,j) = \arctan\left[\frac{\partial f(i,j)}{\partial x} / \frac{\partial f(i,j)}{\partial y}\right], \quad (27)$$

using the approximations $\dfrac{\partial f(i,j)}{\partial x} = f(i+1,j) - f(i-1,j)$ and $\dfrac{\partial f(i,j)}{\partial y} = f(i,j+1) - f(i,j-1)$.

Once the gradient values are obtained, only those pixels that have local maxima along the direction orthogonal to the gradient are chosen by using a non-maximal suppression process which involves interpolating the gradient field. Edges are then identified as those pixels that have a local maximum normal to the gradient direction. Pixels that do not satisfy this criterion are relegated to a NO EDGE (0) set, while those that pass the test are considered as POSSIBLE EDGE (128) candidates. The values in the parentheses correspond to gray level intensities.

As the final step in the process, the possible edges are linked to form a continuous border by implementing a double threshold linking mechanism which involves the user specifying two threshold parameters t_{high} and t_{low}. Let the total number of pixels in POSSIBLE EDGE be N_{edge}.

Then the high threshold t_{high} corresponds to a magnitude level, say Mag_{high} such that

$t_{high} * N_{edge}$ number of pixels have a magnitude less than Mag_{high}, which can be determined

from a magnitude histogram of the POSSIBLE EDGE pixels. Once the high threshold Mag_{high} is

determined, the low threshold is then set to be $Mag_{low} = t_{low} * Mag_{high}$. Any pixel in POSSIBLE

EDGE that has a gradient magnitude greater than Mag_{high} is classified as a valid EDGE (0)

point. Any pixels connected to these valid EDGE points with a gradient value above Mag_{low} are

also classified as EDGE points. In other words, we start from any pixel in POSSIBLE EDGE

and look at its 8-point neighborhood for other POSSIBLE EDGE pixels that satisfy one of the

two criteria stated above. At the conclusion of this step, the algorithm results in an edge map

consisting of EDGE (0) pixels, POSSIBLE EDGE (128) pixels, and NO EDGE (0) pixels.

Selection of suitable values for the threshold parameters t_{high} and t_{low} is critical for a continuous

tracking of edges. For the present application to extract border pixels, a good range of values can

be determined empirically as $0.6 \leq t_{high} \leq 0.9$ and $0.2 \leq t_{low} \leq 0.4$.

The border tracking performance of the above scheme can be illustrated by an

experiment. Fig. 6a shows the input image used for analysis, Fig. 6b shows the edge map

obtained and Fig. 6c shows the thresholded edge map resulting from selection of threshold

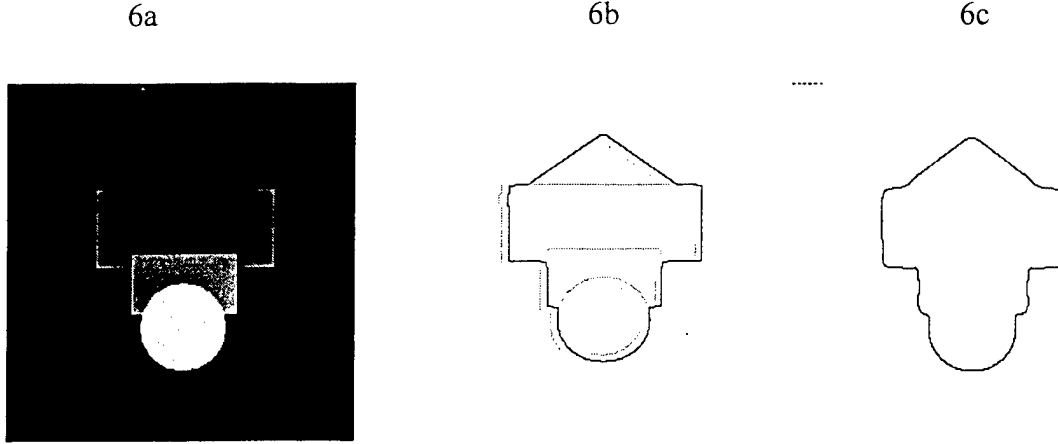parameters $t_{high} = 0.6$ and $t_{low} = 0.2$.

Fig. 6. Border tracking performance:
6a. Input image; 6b. Edge map; 6c. Thresholded edge map.

Once we have the set of border pixels identified, we are ready to proceed with the second stage of the border information modeling. For implementing this stage, we propose a method of modeling the border pixel information as a convex constraint set and subsequenty define a projection operator.

The constraint set is defined as one that enforces a background-foreground separation and can be mathematically formulated as

$$S_{border} = \{ f \in \Xi : \text{foreground of image } f \text{ is bounded by } \xi \} \tag{28}$$

where ξ denotes the set of border pixels. The projection operator associated with this set exists provided if the set is closed and convex, which can be easily ensured if we are dealing with solid convex shapes. The projection operator is then given by

$$P_{border}(f) = f_p \quad \text{where} \quad f_p(i,j) = \begin{cases} f(i,j) : (i,j) \text{ lies inside } \xi \\ 0 \quad : (i,j) \text{ lies outside } \xi. \end{cases} \tag{29}$$

In the case of images that may contain multiple objects, a challenge in the application of the above procedure arises in making a decision on whether a pixel lies inside one of the borders. If one assumes the borders to be convex in shape, any pixel which lies inside the border needs to

be completely surrounded by it, *i.e.* if we move up, down, left, or right from the pixel in question, we are bound to hit the border in any of these directions. This logic may lead to an erroneous result when multiple borders are present, as illustrated in the scenario depicted in Fig. 6. Hence, not only do we need to have intersection with the set of border pixels as we move in all four directions, we should also verify whether all four intersections are occurring with the same set of border pixels. This can be easily handled by assigning a unique label (in the form of gray level intensity) to each of the different sets of border pixels. As illustrated in Fig. 7, the definition of the projection operator characterizes pixel at location P as a valid foreground point whereas both Q and R are set to the background correctly.
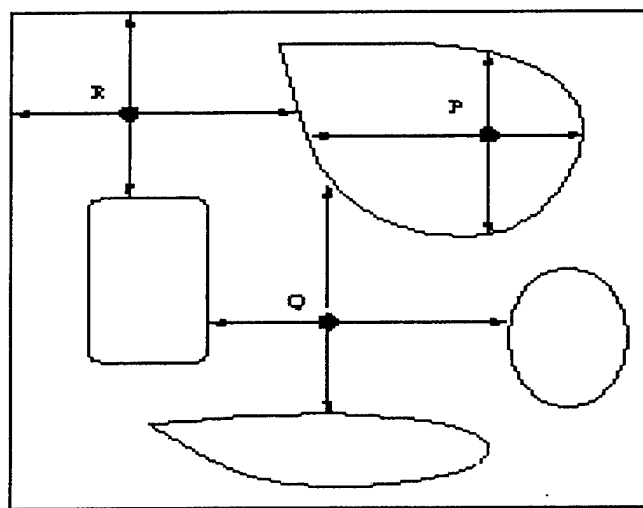

Fig. 7. Projection operation for enforcing border constraint in an image with multiple borders.

To obtain a feel for the extent of restoration and spectrum recovery provided by this constraint set, a controlled experiment was conducted. Fig. 8a shows a simulated image containing multiple objects with different shapes that was blurred by a low pass filtering operation. Fig. 8b shows the blurred image. The loss of spectral content due to blurring can be

seen by comparing Figs. 8c and 8d, which respectively show the spectrum of the original image and its blurred version. The border map obtained from an application of the procedure described above is shown in Fig. 8e. The restored image obtained from a single enforcement of the border constraint is shown in Fig. 8f and the corresponding spectrum is shown in Fig. 8g, which clearly illustrate the restoration and spectrum recovery achieved from this constraint. For obtaining a
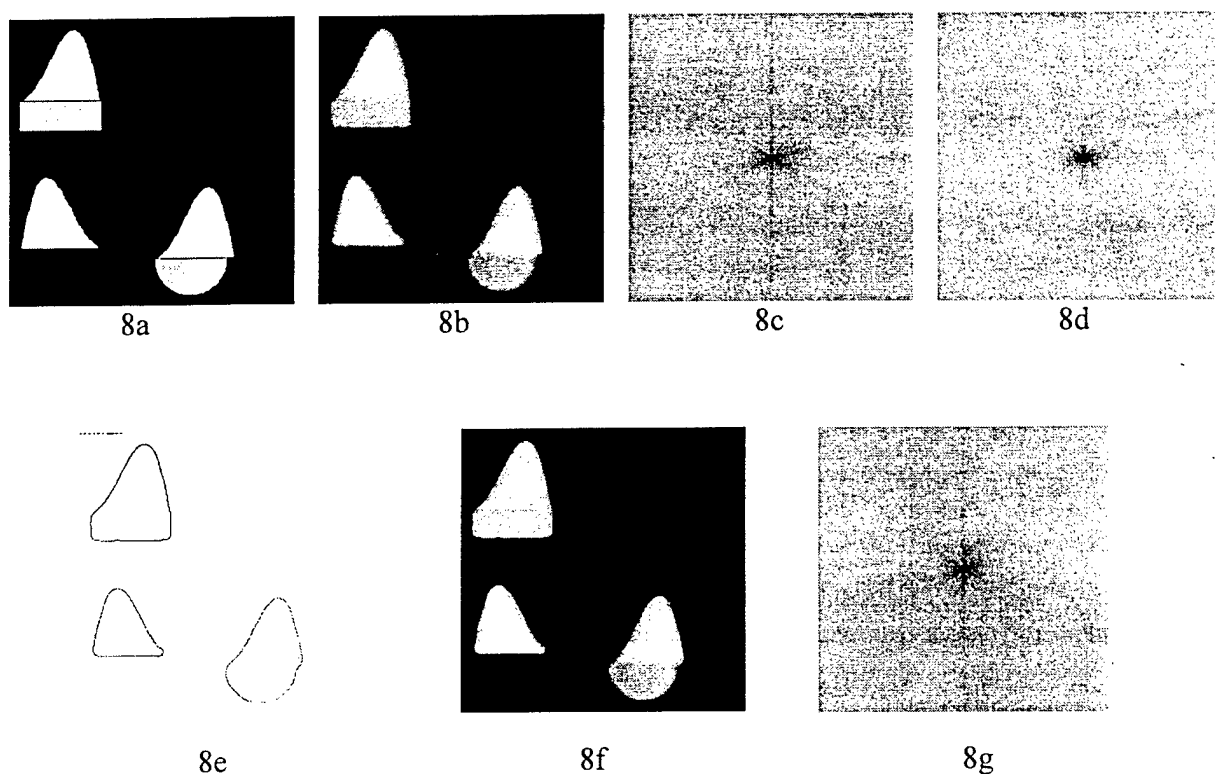

Fig. 8. Restoration and super-resolution of a blurred image using border constraint set 8a. Test image; 8b. Blurred image; 8c. Spectrum of test image; 8d. Spectrum of blurred image; 8e. Output of border extraction filter; 8f. Restored image; 8g. Spectrum of restored image.

quantitative evaluation of the improvement achieved, the L_2-norm of the deviation between the original image and the restored image was computed as 18.69243, which compares favorably with the corresponding deviation between the original image and the blurred image computed as 21.94160. Achievement of this level of restoration from a single application of the constraint is clearly remarkable.

Template Constraint Set

With object border information extracted as above, we cannot restore any non-border edges present in the scene. This is where template-based information modeling becomes useful. A requirement for utilizing this information as a constraint set is the prior knowledge of the presence in the scene of a certain set of templates, a pattern or a sub-image that may occur a multiple number of times in the scene (a right angled corner, circular wheels, etc.). A template matching filter can then give as output the location of the template in the image.

Several procedures for design of template matching filters are discussed in literature. Some early methods, which are quite simple to implement, are based on image subtraction and correlation matching. In one of these methods, the absolute difference between the image and the template is used to determine the template location. While computationally less demanding, this method assumes perfect knowledge of intensity levels and works only in a stationary imaging scenario. Another method, which is more robust to noise and image variations, attempts to construct the filter function that upon convolution with the image containing the template generates maximal response at the template locations. The main drawback in this method however is a lack of proper localization of the template occurrence and the inability to account for the off-center response resulting in broad peaks, which in turn can interfere with accurate localization. A recent and more efficient procedure for designing a template matching filter involves expansion of the image in terms of nonorthogonal basis functions [31], which we propose to employ for identifying template locations and construction of corresponding constraint sets for restoration processing. Matching by expansion is based on expanding the image in terms of basis functions which are all self similar shifted versions of the template. The procedure is briefly outlined in the following.

38

For expanding an image $s(x,y)$ of size $N \times N$ in terms of shifted versions of the template $\phi(x,y)$, one uses the circulant basis functions

$$\psi_{rc}(x,y) = \phi(x-r, y-c), \qquad r,c = 0,1,....,N-1 \qquad (30)$$

in terms of which $s(x,y)$ is estimated in the form

$$\hat{s}(x,y) = \sum_{r=0}^{N-1}\sum_{c=0}^{N-1}\kappa_{rc}\psi_{rc}(x,y) \qquad (31)$$

In (31), κ_{rc} denote the expansion coefficients which are to be found to minimize the deviation between $s(x,y)$ and $\hat{s}(x,y)$. By a lexicographic ordering, $s(x,y)$, $\hat{s}(x,y)$, and $\psi_{rc}(x,y)$ can be expressed as N^2-dimensional vectors $V, \hat{V},$ and Ψ_i respectively in order to formulate the criterion for finding the coefficients κ_{rc} as one of minimizing the squared deviation given by the inner product $<(V-\hat{V}),(V-\hat{V})>$. Now utilizing the orthogonality principle that the approximation error $V - \hat{V}$ is orthogonal to the basis functions, one obtains the N^2 equations

$$<(V-\hat{V}),\Psi_i> = 0, \qquad i = 0,1,2,....,N^2 - 1. \qquad (32)$$

For facilitating the goal of evaluating the expansion coefficients κ_{rc}, these equations can be rewritten more compactly in a matrix form as

$$R_{\psi\psi}K = \Psi V \qquad (33)$$

where $R_{\psi\psi}$ denotes the $N^2 \times N^2$ autocorrelation matrix whose (i,j)-th element is $\langle \Psi_i, \Psi_j \rangle$, $\Psi = [\Psi_0, \Psi_1, ..., \Psi_{N^2-1}]$ and K is a matrix consisting of the expansion coefficients κ_{rc}. If the basis functions selected are linearly independent, $R_{\psi\psi}$ is positive definite and κ_{rc} can be uniquely determined by solving Eq. (33). Solution of Eq. (33) by inverting $R_{\psi\psi}$ is computationally

prohibitive in most cases, and hence Ben-Arie and Rao [31,32] suggested an alternative simpler method obtained by treating the expansion problem as an equivalent deconvolution problem.

For the discrete image $s(x,y)$ of size $N \times N$ to be expanded by a set of self-similar basis functions $\psi_{ij}(x,y)$ as

$$s(x,y) = \sum_{i=-\infty}^{\infty} \sum_{j=-\infty}^{\infty} \kappa_{ij} \psi_{ij}(x,y),$$ (34)

if the basis functions $\psi_{ij}(x,y)$ can be densely arranged in discrete equidistant locations, we have

$$\psi_{ij}(x,y) = \phi(x,y) \otimes \delta(x-i, y-j) = \phi(x-i, y-j)$$ (35)

and hence (34) can be re-written as the discrete convolution

$$s(x,y) = \sum_{i=-\infty}^{\infty} \sum_{j=-\infty}^{\infty} \kappa_{ij} \phi(x-i, y-j) = \kappa(x,y) \otimes \phi(x,y).$$ (36)

The problem of finding the expansion coefficients κ_{ij} can now be handled as reversing the convolution operation in Eq. (36). A particularly simple method is to design a Wiener filter for the case when the image $s(x,y)$ is assumed to contain a noise signal $\lambda(x,y)$, i.e.

$$s(x,y) == \kappa(x,y) \otimes \phi(x,y) + \lambda(x,y).$$ (37)

The Wiener filter is then given by

$$\Theta(\omega_1, \omega_2) = \frac{S_{\kappa s}(\omega_1, \omega_2)}{S_{ss}(\omega_1, \omega_2)}$$

$$S_{\kappa s}(\omega_1, \omega_2) = \Phi(\omega_1, \omega_2) * S_{cc}(\omega_1, \omega_2) \; ; \; S_{ss}(\omega_1, \omega_2) = S_{cc}(\omega_1, \omega_2) \|\Phi(\omega_1, \omega_2)\|^2 + S_{\lambda\lambda}(\omega_1, \omega_2).$$ (38)

In Eq. (38), S_{ss} and $S_{\lambda\lambda}$ respectively denote the spectral densities of the signal $s(x,y)$ and noise $\lambda(x,y)$, and $S_{\kappa s}$ denotes the cross spectral density of $s(x,y)$ and the coefficients $\kappa(x,y)$. $\Phi(\omega_1, \omega_2)$ is the Fourier transform of the template $\phi(x,y)$ and the symbol $*$ denotes conjugation. In an ideal scenario, the discrete function $\kappa(x,y)$ will have a value 1 for

40

$x = x_0, y = y_0$ and will be zero elsewhere. Hence the spectral density of $\kappa(x,y)$ should be a constant, say K_1. Moreover, if the additive noise is assumed to be white gaussian, its power spectral density is also a constant, say K_2. Hence, Eq. (38) can be rewritten as

$$\Theta(\omega_1, \omega_2) = \frac{\Phi(\omega_1, \omega_2)^*}{\left\| \Phi(\omega_1, \omega_2) \right\|^2 + K} \tag{39}$$

where $K = \dfrac{K_1}{K_2}$.

9a   9b   9c
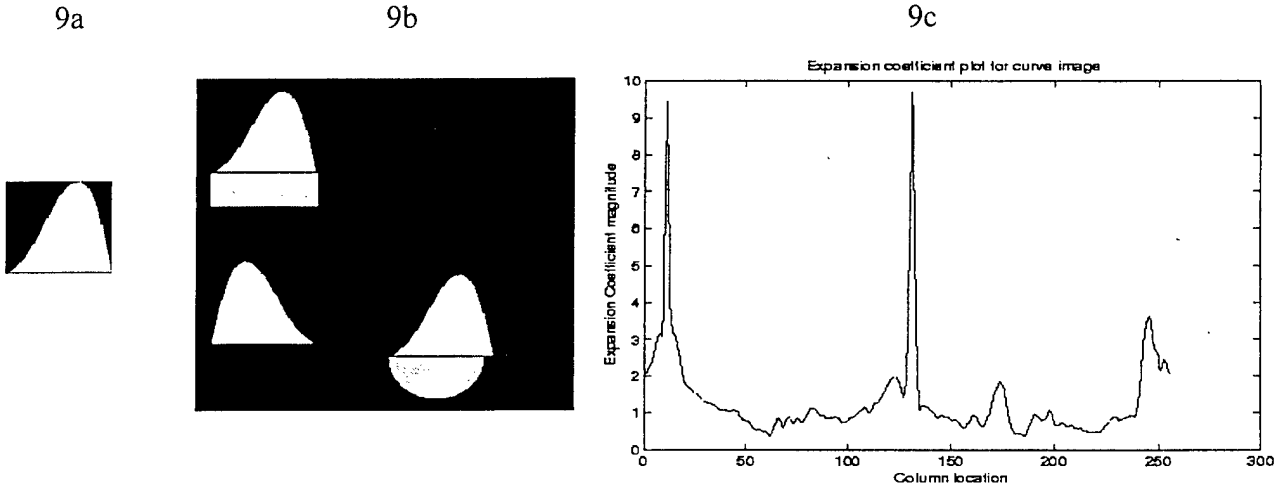

Fig. 9. Template location in a test image
9a. Template; 9b. Test image containing template; 9c. Plot of expansion coefficients

For an illustration of the application of this filter to identify template locations, Fig. 9a shows a template that occurs at two locations (10,10) and (150,130) in the test image shown in Fig. 9b. Fig. 9c shows a plot of the magnitudes of the expansion coefficients in various columns, which correctly depict sharp peaks at the two relevant columns where the template is present.

Once the locations of a template in the image are obtained, one can proceed to design a constraint set and a corresponding projection operator for use in the POCS restoration scheme.

For a template $\phi(i,j)$ of size $m \times m$ identified at the (k,l) pixel location by the filter, the constraint set can be defined as

$$S_{template} = \left\{ f \in \Xi : f(k+i, l+j) = \phi(i,j), \quad \text{where } i,j \in [0,1,2,...,m-1] \right\} \quad (40)$$

$(k,l) \in \left\{ C_{loc} : \text{Set of coordinate locations of the template occurrences} \right\}$.

The projection operator for this set is given by

$$P_{template}(f) = f_p \quad \text{where } f_p(k+i, l+j) = \begin{cases} \phi(i,j) : i,j \in [0,1,2,...,m-1] \} \\ f(i,j) : \text{elsewhere.} \end{cases} \quad (41)$$

The template matching filter as described above performs a binary decision regarding the existence or non-existence of a specific template at a given location in the image, and outputs a peak value at the template location. If multiple templates are present in a given image, a bank of filters, each constructed for a specific template, can be employed in parallel for obtaining the template locations. Alternately, it is possible to modify the filter design such that peaks of different magnitudes corresponding to different templates are obtained in the filter output thus eliminating the need for multiple filters. Details of these modifications are omitted here and can be found in [31,32].

3.3 Restoration of Blurred Images using Scene-derived Constraint sets

In this section we shall briefly describe the restoration and super-resolution performance of two set-theoretic estimation algorithms using the constraint sets developed in the last section by employing a POCS framework. In addition to the two sets S_{border} and $S_{template}$ described by Eqs. (28) and (40), we will use the following three constraint sets:

(i) $S_{mag} = \left\{ f \in \Xi : 255 \geq f(i,j) \geq 0, i,j = 1,2,....N \right\}$ \quad (42)

(ii) $S_{extent} = \left\{ f \in \Xi : f(i,j) = 0 \text{ if } (i,j) \notin \xi \right\}$ \quad (43)

42

and

(iii) $S_{spectrum} = \{ f \in \Xi : F(k,l) = G(k,l), (k,l) \in \zeta \}.$ (44)

While the constraint imposed by S_{mag} is self-explanatory, S_{extent} imposes a spatial extent constraint based on any prior knowledge of a support ξ for the actual image distribution, and $S_{spectrum}$ imposes a constraint in the frequency domain by setting the Fourier transform $F(k,l)$ of the image f equal to the Fourier transform $G(k,l)$ of the original image g within the passband of the sensor ζ. It may be noted that these constraint sets are the ones that have been traditionally employed in POCS-based image reconstruction work in the past [22-24]. The corresponding projection operators can be defined as:

(i) $P_{mag}(f) = f_p$ where $f_p(i,j) = \begin{cases} f(i,j), & \text{if } 0 \leq f(i,j) \leq 255 \\ 0 & , \text{if } f(i,j) \leq 0 \\ 255 & , \text{if } f(i,j) \geq 255. \end{cases}$ (45)

(ii) $P_{extent}(f) = f_p$ where $f_p(i,j) = \begin{cases} f(i,j), & \text{if } (i,j) \in \xi \\ 0 & , \text{if } (i,j) \notin \xi. \end{cases}$ (46)

(iii) $P_{spectrum}(f) = f_p$ where $F_p(k,l) = \begin{cases} G(k,l), & \text{if } (k,l) \in \zeta \\ F(k,l), & \text{if } (k,l) \notin \zeta. \end{cases}$ (47)

These three operators together with the operators P_{border} and $P_{template}$ defined in Eqs. (29) and (41) form the set of operators that will be used in a POCS framework for restoration and super-resolution.

For designing the specific algorithm that employs these constraints one has several options. One option is to use a sequential implementation of the projections P_i at each iteration step as described by Eq. (20) in order to construct the next iterate. Alternately, as noted earlier, one may

use the relaxed projections T_i, constructed from P_i as described in Eq. (21), in a sequential manner to implement the algorithm described in Eq. (22). Improved results together with faster implementation of the algorithm can be obtained from a parallel execution of the projections at each iteration. We shall hence discuss this method in a greater detail in the following.

As noted before, in the traditional implementation of the projections one enforces the constraints in a sequential manner, which in general can result in large computation times, particularly if a number of constraint sets are used. A more efficient implementation will involve employing a parallel processing architecture in which the projections onto the different constraint sets at each iteration can be simultaneously executed and the next iterate is computed as a weighted sum of these projections. One version of this approach, popularly referred to as the Method of Parallel Projections (MOPP) [33,34], has been found in our investigations to possess attractive convergence properties. In this scheme, an elementary iteration consists in projecting the current estimate simultaneously onto selected sets and forming a relaxed convex combination of the projections.

For a brief description of the method, given the image to be restored, denoted as the starting image $\hat{f}(0)$ for commencing the POCS iterations, and two numbers $\varepsilon \in (0,1)$ and M a positive integer, MOPP implements the recursion

$$\hat{f}^{(n+1)} = \hat{f}^{(n)} + \lambda_n \left[\sum_{i \in I_n} w_{i,n} P_{i,n}(\hat{f}^{(n)}) - \hat{f}^{(n)} \right] \tag{48}$$

together with the following conditions:

(i) $\lambda_n \in [\varepsilon, 2 - \varepsilon]$ and (ii) $\sum_{i \in I_n} w_{i,n} = 1$, where $0 \neq I_n \subset I$ and $I \subset \bigcup_{k=0}^{M-1} I_{n+k}$,

I denoting the set of constraints used.

44

For demonstrating the restoration performance of the MOPP algorithm, we shall present the results of a simulation experiment in Figs. 10a-b. The blurred image to which the method was applied is shown in Fig. 10a and its restored version after 20 iterations of MOPP algorithm using the border and template constraint sets is shown in Fig. 10b. The normalized proximity measure given by Eq. (8) was used as the performance measure.

10a   10b

Fig 10. Restoration of a blurred image with MOPP algorithm
10a. Blurred image; 10b. Restored image

4 A HYBRID SUPER-RESOLUTION ALGORITHM COMBINING POCS AND ML APPROACHES

It is evident from the discussion in the last section that the POCS approach provides an attractive alternative to the statistical optimization approach for restoring degraded images. In particular, for super-resolving poorly acquired images by the POCS approach the flexibility offered for constructing constraint sets and utilizing them during processing is particularly noteworthy. It is to be noted that the types of information used in the restoration, *viz.* border constraints and template constraints, are not possible to utilize during implementation of algorithms derived following statistical optimization-based approaches, for instance during execution of ML super-resolution algorithm discussed in Section 2. However, statistical optimization methods in general, and ML algorithm in particular, have a number of advantages (as discussed before) which one may not like to sacrifice. The strong points of these two complementary approaches can be combined to produce hybrid schemes that offer very attractive restoration and super-resolution performance. Two such hybrid algorithms will be presented in this section.

4.1 POCS-assisted ML algorithm

In this scheme, we implement the ML iterations given by Eq. (2) as the main image restoration scheme and include a POCS adjustment of the ML estimate for enforcing constraints after every cycle of ML iterations is completed. More specifically, we execute L iterations of POCS adjustment after each cycle of K iterations of the ML algorithm. Thus, each iteration cycle of the combined algorithm applies an ML iteration cycle comprising K number of ML iterations followed by a POCS adjustment cycle comprising L number of POCS iterations. The combined algorithm is run for a total of N iterations. It is easy to see that

this algorithm in effect performs a constrained maximization of the likelihood function in an iterative manner. The implementation details are summarized in the following table.

1. *Read the blurred image data (g).*
2. *Set initial conditions to commence ML iterations, $\hat{f}_0 = g$.*
3. *Perform ML restoration implementing the updating algorithm given in Eq. (2).*
4. *Compute the likelihood and l_2-norm values at the end of each iteration.*
5. *Repeat steps 3-4 for K iterations.*
6. *Perform POCS adjustment using MOPP scheme and implementing updating algorithm given in Eq. (48).*
7. *Repeat step 6 for L iterations.*
8. *Repeat steps 3-6 for N iterations.*
9. *Save processed image and compute likelihood and l_2-norm values.*

Table 1.   Simulation Flow of POCS-assisted ML Algorithm

For evaluating the performance of this new algorithm, we conducted a number of simulation experiments. The results of one experiment will be briefly described. In this experiment, the POCS-assisted ML algorithm was used to restore the blurred image shown in Fig. 10a by employing the same two constraints as discussed in the last section (*viz.*, Border Constraint and Template Constraint) for POCS adjustment. The algorithm was implemented with values of $K=5$ and $N=3$ (K being the number of ML iterations executed before a POCS adjustment and N being the total number of iterations for the combined cycle). However, we varied the value of L, the number of POCS adjustment iterations within each cycle from two to ten and examined the effect it has on the performance of the ML algorithm. Figs. 11a and 11b respectively show plots of the variation of the likelihood function and the l_2-*norm* of restoration error computed in the spatial domain against the total number of ML iterations executed with the value of L varied from $L = 0$ (pure ML algorithm with no POCS adjustments) to $L = 2$, 6, and 10. It is evident that the hybrid scheme outperforms the ML algorithm without any POCS adjustments. An item of special interest to note is the jump in the likelihood function as the algorithm switches from ML

iteration cycle to the POCS adjustment cycle. A corresponding fall in the l_2-norm of the restoration error is also observed at these points. Furthermore, the amount of increase in the likelihood (and the decrease in l_2-norm of the restoration error) improves with the number of iterations of POCS (i.e. value of L) executed. However, it is also interesting to see that most of the improvement due to the inclusion of POCS adjustments comes during the first few iterations of POCS and beyond that there is not much change in the performance.
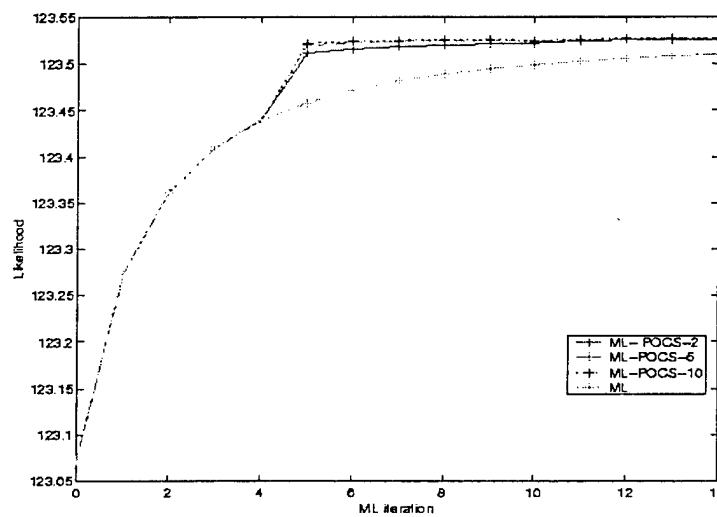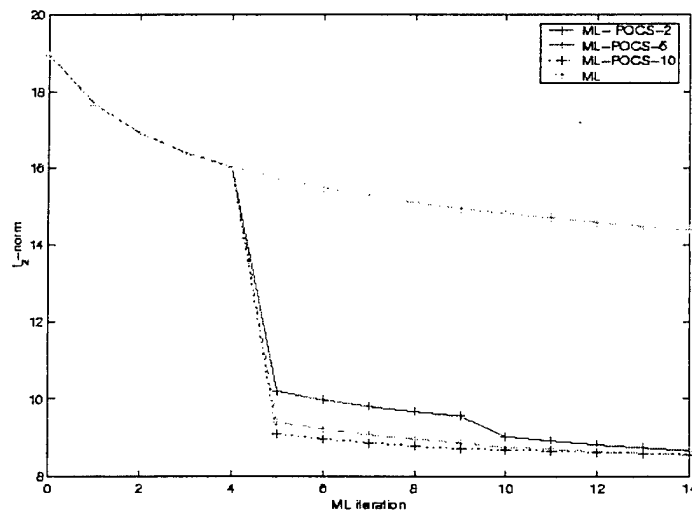

Fig. 11a. Plot of Likelihood Values

Fig. 11b. Plot of l_2-norm of Restoration Error

48

4.2 ML-assisted POCS algorithm

An alternate way of creating a hybrid restoration algorithm is to use POCS updating as the main restoration scheme and employ execution of ML updating for the intermediate adjustment steps. We shall refer to this algorithm as ML-assisted POCS algorithm in further discussion. More specifically, we execute K iterations of ML adjustment after each cycle of L iterations of the POCS adjustment implemented using the MOPP approach as in Eq. (48). Thus, each iteration cycle of the combined algorithm now applies a POCS iteration cycle comprising L number of POCS iterations (implementing the updating in Eq. (48)) followed by a ML adjustment cycle comprising K number of ML iterations (implementing the updating in Eq. (2)). The combined algorithm is run for a total of N iterations. The implementation details are summarized in the following table.

1.	*Read the blurred image data (g).*
2.	*Set initial conditions to commence POCS iterations, $\hat{f}_0 = g$.*
3.	*Perform POCS restoration using MOPP framework and adaptive relaxation implementing the updating algorithm given in Eq. (48).*
4.	*Compute the likelihood and l_2-norm values at the end of each iteration.*
5.	*Repeat steps 3-4 for L iterations.*
6.	*Perform ML adjustment implementing updating algorithm given in Eq. (2).*
7.	*Repeat step 6 for K iterations.*
8.	*Repeat steps 3-6 for N iterations.*
9.	*Save processed image and compute likelihood and l_2-norm values.*

Table 2. Simulation Flow of ML-assisted POCS Algorithm

The performance of this algorithm was also evaluated by applying it to the same restoration problem discussed earlier of restoring the blurred image shown in Fig. 10a. The POCS updating was implemented by employing the same two constraints as discussed in the last section (*viz.,* Border Constraint and Template Constraint). The algorithm was implemented with values of $L=5$ and $N=3$ (L being the number of POCS iterations executed before a ML adjustment and N being

the total number of iterations for the combined cycle). In this case, the value of K, the number of ML adjustment iterations within each cycle, was varied to examine the effect it has on the performance of the POCS restoration. Figs. 12a and 12b respectively show plots of the variation of the normalized proximity measure (computed as in Eq. (23)) and of the l_2-*norm* of restoration error computed in the spatial domain against the total number of POCS iterations executed with the value of K varied from $K = 0$ (pure POCS algorithm with no ML adjustments) to $K = 2$, and 5. Once again it is evident that the hybrid scheme outperforms the POCS iteration scheme without the ML adjustments. Of particular interest is to note the downward break in the two plots as the algorithm switches from the POCS iteration cycle to the ML adjustment cycle. Furthermore, the amount of performance improvement increases with the number of iterations of ML adjustment (*i.e.* value of K) executed between two POCS cycles.
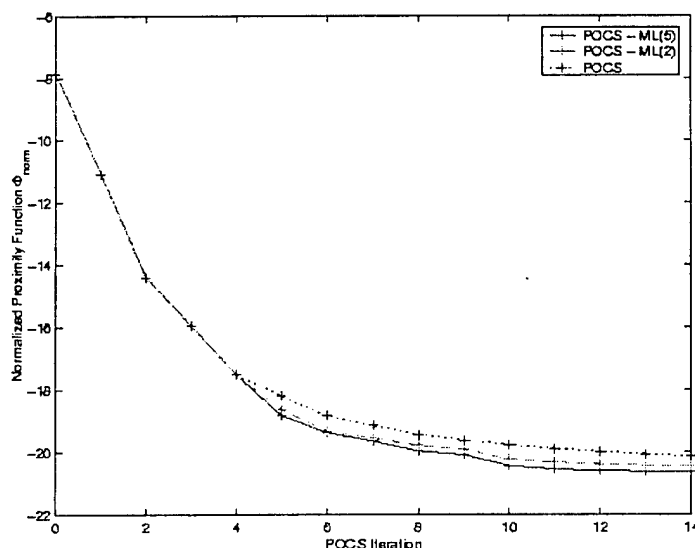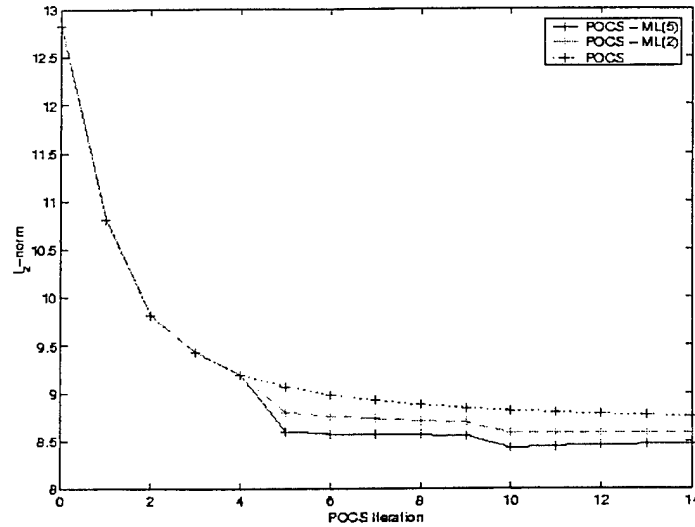

Fig. 12a. Plot of Proximity Measure

50

Fig. 12b. Plot of l_2-norm of Restoration Error

Hoe does this algorithm compare with the other hybrid algorithm presented earlier? To answer this question, an examination of the l_2-norm plots in Figs. 11b and 12b can be made since the same blurred image was processed by the two algorithms using the same sets of parameters. At the end of 15 iterations of the main restoration algorithm, the ML-assisted POCS yielded a smaller value of the restoration error than the POCS-assisted ML algorithm. The latter algorithm started with a larger initial error but the POCS adjustment step caused a sharper decay in the error compared to that produced by the ML adjustment step in the ML-assisted POCS algorithm. One should also take into consideration that the ML-assisted POCS algorithm required more computation time for the same number of iterations than the other scheme. Thus in practical implementations where processing time (and hence the number of frames that can be processed within a given time) is of particular concern, one may prefer the POCS-assisted ML algorithm over the other hybrid scheme. On the other hand, when quality of the final restored image is of importance, the ML-assisted POCS algorithm seems to be a better choice.

51

4.3   Application of POCS-Assisted ML Algorithm to Restoration of PMMW Images

An application of POCS-assisted ML algorithm has been made to the super-resolution of

PMMW images with significant performance improvements noted in comparison to the

application of ML algorithm. For providing an illustration of this, we show in Fig. 13a a PMMW

image, popularly referred to as "Pattern Image", collected by a 95 GHz camera with a 3 *in*

lens/horn built at the Army Research Laboratory (ARL) at Adelphi, MD. This image, of size

65×33 pixels, has over the years become a sort of benchmark image for testing the performance

of different super-resolution algorithms. More details on this data can be found in various ARL

publications, one of which is the recent paper by Silverstein [18].

Fig. 13b shows the restored image after 15 iterations of the ML algorithm. The application of

the POCS-assisted ML algorithm to the same image with 5 ML iterations and 3 POCS

adjustments alternately implemented for 2 cycles (i.e. $K = 5$, $L = 3$, and $N = 2$) resulted in a

restored image shown in Fig. 13c. Comparing the images in Figs. 13b and 13c, one may note the
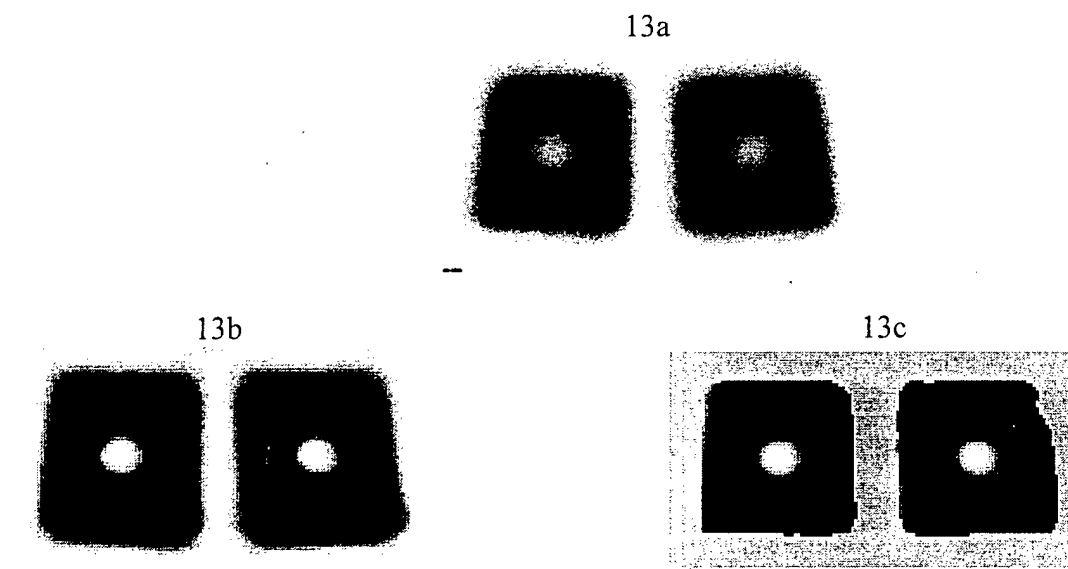

*Fig. 13. Results of processing PMMW "pattern" image by ML and POCS-assisted ML
algorithms.
13a. Acquired Image; 13b. ML Processed Image; 13c. Image processed by POCS-assisted ML*

superior edge restoration and the absence of processing artifacts, which clearly illustrate the strengths of the present hybrid algorithm. It is to be noted that these performance gains have resulted in addition to a reduction in the total number of ML iterations (only 10 in POCS-assisted ML compared to 15 in ML), which is the more computationally expensive part of the super-resolution process.

As a further comparison of the super-resolution performance, the spatial frequency distribution plots were also compared. Fig. 14 shows the variation of the normalized intensity (in dB) plotted as a function of the frequency for a cut through the spectrum of the acquired image (shown in dotted lines) and also the corresponding variations for the ML processed image (shown in dark solid line) and for the POCS-assisted ML processed image (shown in fainter solid line). It is easy to see that while the ML algorithm has recovered some frequencies beyond the passband of the sensor, the recovery of spectral components by the POCS-assisted ML algorithm is significantly more extensive.

As a final illustration of the performance of the POCS-assisted ML algorithm in super-resolving PMMW images, we show in Fig. 15 below the restoration of the "Tank" image discussed earlier in Section 2. This is a resultant of processing with the POCS-assisted ML algorithm using 5 ML iterations alternating with 5 POCS adjustment iterations implemented for 3 cycles, which corresponds to a computation time roughly equivalent to that required to execute 15 ML iterations. Comparing the restoration obtained here with that shown in Fig. 4c, which is the restored image after 100 ML iterations, one can clearly appreciate the benefits resulting from the hybrid approach presented in this work.
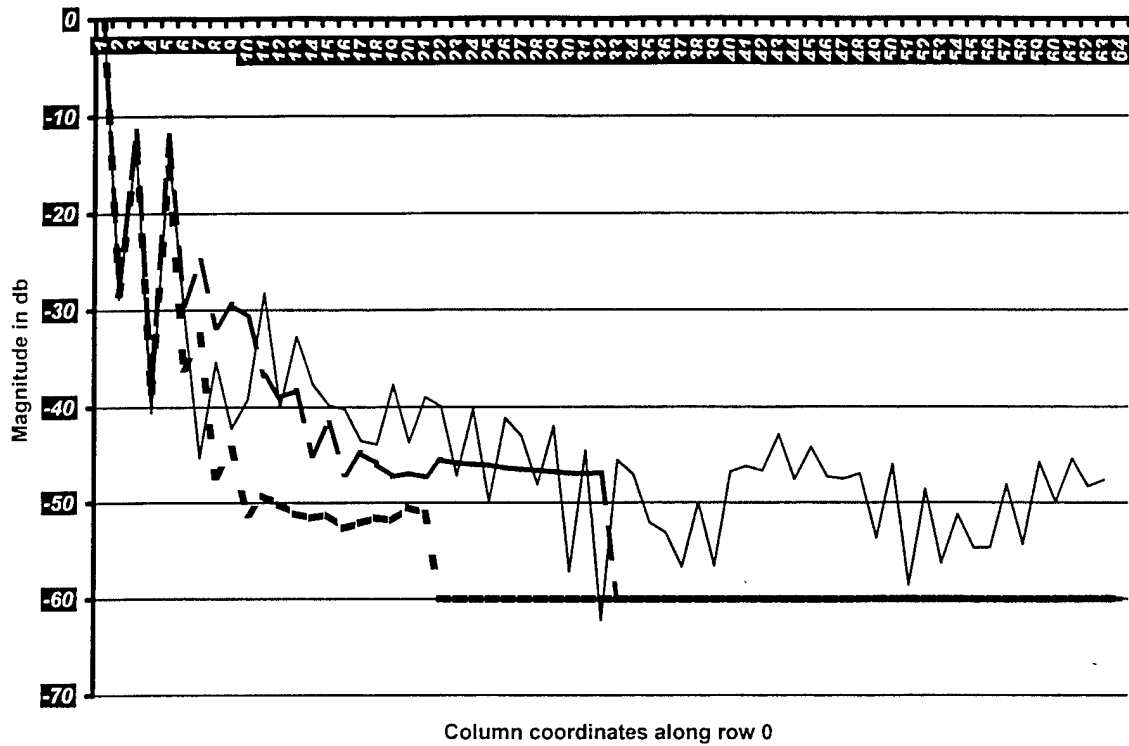
Spectral Data(ARL "Pattern" Benchmark)

Fig.14. Comparison of spatial frequency spectra of processed and unprocessed images (Dotted line – original blurred image; Dark solid line – restoration by ML algorithm; Fainter solid line – restoration by POCS-assisted ML algorithm)
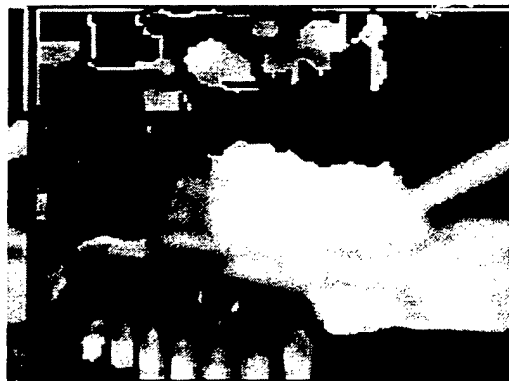

Fig. 15. Restoration of "Tank" image by POCS-assisted ML algorithm

54

5. CONCLUSIONS

The major contributions from this project are the development of scene-based information sets for use as constraints within a set-theoretic estimation framework for image restoration and the design of two new hybrid algorithms, called POCS-assisted ML algorithm and ML-assisted POCS algorithm. These algorithms, which iteratively apply a cycle of ML estimation iterations followed by a cycle of POCS adjustment iterations, combine the strong points of the two approaches and hence possess a number of implementation benefits. For facilitating the POCS adjustment, two novel information sets that may be derived from the image being processed were also developed. These sets, together with the traditionally applied constraints, such as non-negativity of intensity, spatial extent of objects, and noise variance, provide a rich set of information constraints that can be advantageously utilized to speed up the convergence of the ML estimation process. Several experimental results were presented to describe the performance of the new algorithms in super-resolving PMMW images. The superior restoration of the object features observed in the image domain and the significant extrapolation of spatial frequencies observed in the spectral domain lead us to conclude that the POCS-assisted ML algorithm and the ML-assisted POCS algorithm are perhaps the most powerful super-resolution algorithms available today for restoration of imagery acquired from diffraction-limited sensing operations.

REFERENCES

1. A. K. Jain, *Fundamentals of Digital Image Processing,* Prentice-Hall, 1989.

2. J. Goodman, *Introduction to Fourier optics,* McGraw-Hill, 1996.

3. C.K. Rushforth and J.L. Harris, "Restoration, Resolution and Noise", *J. of Optical Society of America,* Vol. 58, pp. 539-545, 1968.

4. R.W. Gerchberg, "Super-resolution through error energy reduction", *Optica Acta,* Vol. 21, pp. 709-720, 1974.

5. A. Papoulis, "A new algorithm in spectral analysis and band-limited extrapolation", *IEEE Trans. on Circuits and Systems,* Vol. CAS-22, pp. 735-742, 1975.

6. J. Biemond, R.L. Lagendijk and R.M. Mersereau, "Iterative methods for image deblurring", *Proc. of IEEE,* Vol. 78, pp. 856-883, 1990.

7. M. I. Sezan and A.M. Tekalp, "Survey of recent developments in digital image restoration", *Optical Engineering,* Vol. 29, pp. 393-404, 1990.

8. W. H. Richardson, "Bayesian-based iterative method of image restoration", *Journal of the Optical Society of America,* Vol. 62, pp 55-60, 1972.

9. L. B. Lucy, "An iterative technique for the rectification of observed distribution", *Astronomical Journal,* Vol. 79, No 6, pp 745-59, June 1974.

10. M. K. Sundareshan, "Super-resolution processing and fusion of multi-sensor data for advanced target surveillance and tracking", *Final Report submitted to AFOSR (Grant # F49620-97-1-0243),* AFOSR/NM, Arlington, VA, May 2000.

11. B. R. Hunt, " Imagery super-resolution: emerging prospects", *Proc. of 1991 SPIE conf. on Applications of Digital image Processing XIV,* San Diego, CA, Vol. 1567, pp 600-608, 1991.

12. B. R. Hunt, "Super-resolution of images: algorithms, principles and performance", *International Journal of Imaging Systems and Technology,* Vol. 6, pp 297-304, 1995.

13. E. Levitan and G. T. Herman, " A maximum *a posteriori* probability expectation maximization algorithm for image reconstruction in emission tomography", *IEEE Transactions on Medical Imaging,* Vol. MI-6, pp 185-192, 1987.

14. H. Pang, M. K. Sundareshan and S. Amphay, "Super-resolution of millimeter-wave images by iterative blind maximum likelihood restoration", *Proc. of 1997 SPIE Conf, on Passive Millimeter Wave Imaging Technology,* Orlando, Florida, Vol. 3064, pp 227-38, April 1997.

15. H. Pang, M. K. Sundareshan and S. Amphay, "Optimized maximum likelihood algorithms for super-resolution of passive millimeterwave imagery", *Proc. of SPIE Passive Millimeter Wave Imaging Technology Conference (Aerosense'98)*, Orlando, Florida, Vol. 3378, pp 148-160, April 1998.

16. A. M. Darling, T. J. Hall and M. A. Fiddy, "Stable non-iterative object reconstruction from incomplete data using *a priori* knowledge", *J. of Optical Society of America*, Vol. 73, pp 1466-1469, 1983.

17. D. O. Walsh and P. A. Nielsen-Delaney, "Direct method for super-resolution", *Journal of Optical Society of America A*, Vol. 11, pp 572-579, 1994.

18. J. D. Silverstein, " Passive millimeter-wave image resolution improvement by linear and nonlinear algorithms", *Proc. of SPIE Passive Millimeter Wave Imaging Technology Conference (Aerosense'2001)*, Orlando, Florida, Vol. 4373, April 2001.

19. L. M. Bergman, " The method of successive projections for finding a common point of convex sets", *Soviet Math. Dokl.*, Vol. 6, No.3, pp. 688-692, 1965.

20. L. G. Gubin, B. T. Polak, and E. V. Raik, " The method of projection for finding the common point of convex sets", *USSR Comput. Math. and Math. Physics*, Vol. 7, No. 6, pp. 1-24, 1967.

21. A. Lent and H. Tuy, " An iterative method for extrapolation of band-limited functions", *Journal of Math. Anal. And Applications*, Vol. 83, pp. 544-565, 1981.

22. D. C. Youla, "Generalized image restoration by the method of alternating orthogonal projections", *IEEE Transactions on Circuits & Systems*, Vol. 25, No. 9, pp 694-702, September 1978.

23. D. C. Youla and H. Webb, "Image restoration by the method of convex projections: Part 1 - theory", *IEEE Transactions on Medical Imaging*, Vol. M1-1, No 2 pp 81-94, October 1982.

24. M. I. Sezan and H. Stark, "Image restoration by the method of convex projections: Part 2 - Application and numerical results", *IEEE Transactions on Medical Imaging*, Vol. M1-1, No 2 , pp 95-101, October 1982.

25. H. J. Trussell and M. R. Civanlar, " Feasible solution in signal reconstruction", *IEEE Transactions on acoustics, speech and Signal Processing*, Vol. ASSP-32, No. 2, pp201-212, April 1984.

26. P. L. Combettes, "The foundations of set theoretic estimation", *Proceedings of the IEEE*, Vol. 81 No 2, pp 182 -208, February 1993.

27. H. Stark (Ed), *Image Recovery: Theory and Application*, Academic Press, San Diego, 1987.

28. M. I. Sezan, "An overview of convex projections theory and its application to image recovery problems" , *Ultramicroscopy,* Vol. 40, pp 55-67, 1992.

29. I. Sacolick, "Reconstructing animations from motion-corrupted MRI using POCS algorithm", *M. S. Thesis*, ECE Department, Univ. of Arizona, 1996.

30. J. Canny, "A computational approach to edge detection", *IEEE Transactions on Pattern Analysis and Machine Intelligence,* Vol. PAMI-8, No. 6, November 1986.

31. J. Ben-Arie and K. R. Rao, "A novel approach for template matching by nonorthogonal image expansion", *IEEE Transactions on Circuits and Systems for Video Technology,* Vol. 3, No. 1, pp 71-84, 1993.

32. K. R. Rao and J. Ben-Arie, "Multiple template matching using the expansion filter", *IEEE Transactions on Circuits and Systems for Video Technology,* Vol. 4, No. 5, pp 490-503, 1994.

33. P. L. Combettes, "Iterations of parallel convex projections in Hilbert spaces", *Numerical Functional Analysis and Optimization*, Vol. 15, No 3, pp 225-43, 1994.

34. P. L. Combettes, "Parallel projection method for set theoretic signal reconstruction and restoration", *Proceedings of IEEE International Conf. on Acoustics, Speech and Signal Processing*, pp 297-300, 1993.

35. M. K. Sundareshan, "Performance of iterative and non-iterative schemes for image restoration and super-resolution processing in multi-spectral seeker environments", *Final Report for AFOSR Summer Research Program*, AFOSR SREP-1, Feb. 1997.